STUDIES DEFINING THE ROLE OF PROTEIN DISULFIDE ISOMERASE-9 IN POLLEN BIOGENESIS IN *ARABIDOPSIS THALIANA*

A THESIS SUBMITTED TO THE GRADUATE DIVISION OF THE

UNIVERSITY OF HAWAIʻI AT MĀNOA IN PARTIAL FULFILLMENT OF THE

REQUIREMENTS FOR THE DEGREE OF

MASTER OF SCIENCE

IN

MOLECULAR BIOSCIENCES AND BIOENGINEERING

MAY 2019

By

Elizabeth M. Feldeverd

Thesis Committee:

David Christopher, Chairperson

Jon-Paul Bingham

Daniel Owens

Keywords: protein disulfide isomerase, pollen, heat stress, unfolded protein response

ACKNOWLEDGEMENTS

My thesis work would not be possible without the help of many people. I have received immense support throughout my research and, more broadly, in my development as a scientist.

First and foremost, I would like to acknowledge my principal investigator Dr. David Christopher. I am sincerely grateful for his mentorship and the opportunity to work on this project. My committee members, Drs. Jon-Paul Bingham and Daniel K. Owens, have each provided invaluable guidance during my time at the University of Hawai‘i at Mānoa.

There are several other people who have made this work possible. I would like to thank fellow laboratory members Dr. Christen Yuen, Kristie Matsumoto, and Rina Carrillo for their feedback and support. Tina Weatherby Carvalho at the Biological Electron Microscope Facility provided training on the laser scanning confocal microscope(s) and scanning electron microscope. Additionally, Dr. Maarit Tiirikainen at the UH Cancer Center processed quantitative real-time PCR samples.

ABSTRACT

Protein disulfide isomerases (PDIs) are disulfide bond catalysts that serve a breadth of important roles in eukaryotic growth and development. *Arabidopsis thaliana* has fourteen PDIs with variations on the canonical domain arrangement and subcellular location. Among them, *PDI9* and its homolog *PDI10* are part of the unfolded protein response (UPR) and have been shown to fold proteins via disulfide bonds. Using a PDI9-specific antiserum, PDI9 was found to be expressed in mature pollen. Here, the role of *PDI9* in pollen biogenesis was characterized on molecular and cellular scales. First, using transfected leaf mesophyll protoplasts, PDI9 was shown to co-localize in the endoplasmic reticulum with two proteins (Leucine Rich Repeat-Extensin 8, LRX8, and ER Membrane Complex Subunit 7, EMC7) that are both expressed in pollen. Double knockout *pdi9-pdi10* seedlings were used to demonstrate constitutive up-regulation of other PDIs and chaperones in non-UPR-stressed conditions relative to wild-type. Using an improved high-throughput Alexander staining method and scanning electron microscopy, *PDI9* was found to play a crucial role in pollen development under prolonged heat stress. The single *pdi9* and double *pdi9-pdi10* knockout plants produce less viable pollen, dehisce fewer pollen grains, have impaired silique development, and exine formation is severely disrupted. Taken together, these data suggest that PDI9 mediates the development of healthy pollen under heat stress via its role in the UPR and its interactions with secretory substrates (LRX8, EMC7).

Contents

LIST OF TABLES 5
LIST OF FIGURES 6
ABBREVIATIONS 7
CHAPTER I: INTRODUCTION AND BACKGROUND 8
Structure and function of protein disulfide isomerases 8
Proteostasis and the Unfolded Protein Response (UPR) 11
Functions and phenotypes of protein disulfide isomerase in mammals 17
PDI and thioredoxin-like proteins in yeast and *E. coli* 20
Complementation and redundancy of protein disulfide isomerase 21
PDIs in plants 22
Plant reproduction and proteostasis 27
PDI9 and its potential interactors 31
CHAPTER II: RATIONALE, HYPOTHESES, AND OBJECTIVES 37
Significance of work *37*
Research questions and hypotheses *39*
Objectives 41
CHAPTER III: CO-LOCALIZATION OF PROTEINS IN TRANSFECTED PROTOPLASTS 43
Introduction 43
Methods 44
Construct design and plasmid subcloning 44
Protoplast transfection and laser scanning confocal microscopy 47
Results 48
EMC7 and PDI9 co-localization 48
LRX8 and PDI9 co-localization 50
Discussion 52
CHAPTER IV: CHARACTERIZATION AND EXPRESSION ANALYSIS OF UPR GENES IN A *PDI9-PDI10* MUTANT 54
Introduction 54
Methods 55
Authenticating previously created *PDI9* and *PDI10* mutants 55
Quantitative PCR (qPCR) of UPR genes in chemically-stressed seedlings 57
Results 60

Genotyping and RT-PCR of *PDI9* and *PDI10* mutants 60
qPCR of UPR transcripts in ER-stressed seedlings 61
Discussion 62
CHAPTER V: HEAT STRESS PHENOTYPING OF REPRODUCTIVE TISSUES OF *PDI9* AND *PDI10* MUTANTS 65
Introduction 65
Methods 67
Characterizing PDI9 expression in floral tissues 67
Heat stress treatment 67
High-throughput pollen viability assay using a modified Alexander stain 68
Heat-stressed pollen scanning electron microscopy 71
Heat-stressed silique phenotyping 71
Results 73
Western blotting of floral proteins from select *PDI9* mutants 73
High-throughput Alexander staining of heat-stressed pollen 74
SEM of heat-stressed pollen 77
Heat-stressed siliques 82
Discussion 84
Pollen viability and pollen counts 84
Pollen morphology and exine patterning 84
Heat-stressed silique development 85
Conclusions 86
REFERENCES 88
APPENDIX: LIST OF PRESENTATIONS 99

LIST OF TABLES

TABLE 1: Known plant transcription factors and their characteristics 13
TABLE 2: *Arabidopsis thaliana* protein disulfide isomerases and their characteristics. 24
TABLE 3: Primer sequences for genotyping and RT-PCR 57
TABLE 4: Primers for qPCR 58
TABLE 5: The normalized expression (%) of given UPR transcripts relative to housekeeping gene (HKG) Actin2 for given genotype-treatment 61
TABLE 6: Comparison of pollen viability staining methods 68
TABLE 7: The number of dehisced pollen grains for each genotype-treatment 75

LIST OF FIGURES

FIGURE 1: The ribbon structure of yeast PDI showing the classical a-b-b'-a' domain arrangement with its C-terminal helix domain. 10

FIGURE 2: RNA blots of *AtPDI* mRNAs after treatment with tunicamycin (Tm). 14

FIGURE 3: Transfected mesophyll protoplasts show PDI9 and PDI10 co-localize with the ER and form punctate structures 26

FIGURE 4: Pro_{PDI9}:GUS fusion shows *PDI9* is highly expressed in mature anthers and pollen. 26

FIGURE 5: Angiosperm pollen cell wall structure. 28

FIGURE 6: Expression of UPR-related genes during pollen development and germination. 30

FIGURE 7: Domain arrangements of two potential PDI9 interactors. LRX8 (top) and EMC7 (bottom) .. 32

FIGURE 8: Triple and quadruple knockout mutants of the pollen *LRX* family members (*LRX8-11*) have significantly reduced seed set. 33

FIGURE 9: Plasmid design for co-localization experiments showing the restriction sites used on pBluescript ks+ and the gene of interest (*LRX8*, *EMC7*). 44

FIGURE 10: EMC7:mCherry partially co-localizes with PDI9:eGFP and shows ER/cis-Golgi labeling. 48

FIGURE 11: EMC7:mCherry localization shows a distinct secondary subcellular location. 49

FIGURE 12: LRX8 and PDI9 co-localization in transfected protoplasts. 50

FIGURE 13: LRX8 co-localizes with PDI2, an ER-resident protein 51

FIGURE 14: T-DNA insertions for *pdi9-1, pdi9-2*, and *pdi10-1* mutants. 56

FIGURE 15: Primer locations for *bZIP60* unspliced *(bZIP60u)* and spliced *(bZIP60s)*. 59

FIGURE 16: Characterization of *PDI9* and *PDI10* genotypes 60

FIGURE 17: Western blotting of floral tissues with PDI9 antiserum. 73

FIGURE 18: *PDI9* is critical for the development of viable pollen under heat stress. 74

FIGURE 19: Scanning electron micrographs of pollen grains. 77

FIGURE 20: Scanning electron micrographs of pollen exine patterning. 79

FIGURE 21: Addition scanning electron micrographs of representative *PDI9* OE pollen 80

FIGURE 22: Representative anthers from (A) wild-type and (B) DKO heat-stressed flowers. 80

FIGURE 23: Heat-stressed DKO pollen within (A) anthers and (B) dehisced. 81

FIGURE 24: Representative siliques from control and heat-stressed plants 82

FIGURE 25: Silique length of control and heat-stressed plants. 83

ABBREVIATIONS

ANOVA- Analysis of variance

B-ME- Beta-mercaptoethanol

Co-IP- Co-immunoprecipitation

DTT- dithiothrietol

EMC- Endoplasmic reticulum membrane protein complex

ER- Endoplasmic reticulum

ERAD- Endoplasmic reticulum associated degradation

PCR- Polymerase chain reaction

PDI- Protein disulfide isomerase

UPR- Unfolded protein response

TF- Transcription factor

Tm- Tunicamycin

TMD- Transmembrane domain

UPR - Unfolded protein response

CHAPTER I: INTRODUCTION AND BACKGROUND

Structure and function of protein disulfide isomerases

The endoplasmic reticulum (ER) is a membranous structure connected to the nuclear envelope responsible for secretory protein synthesis, catalyzing proper folding of nascent proteins and initiating their secretion in all eukaryotic cells. Its network of tubules and sacs expands throughout the cell. The intramembrane space known as the ER lumen takes up as much as ten percent of the cell volume (Alberts et al. 2002). The ER is the gateway to the secretory protein pathway in plant cells. About one-third of all proteins are secreted or are membrane proteins that are folded and assembled in the ER (Ron and Walter 2007). Plant development and extracellular communication are inexorably linked to the secretory protein pathway.

Protein folding is a dynamic process involving ionic, hydrophobic and covalent interactions among amino acids to produce a native three-dimensional protein. It is also an error-prone process that is counter-acted by molecular chaperones and foldases within the ER that help proteins reach their correct functional conformation. Molecular chaperones help prevent premature or incorrect folding of substrates, whereas foldases accelerate the correct folding of substrates. Protein disulfide isomerases (PDI) are ubiquitous proteins found in all eukaryotes that may have both chaperone and foldase activities. PDIs catalyze the creation, isomerization and breakage of disulfide bonds on substrate polypeptides. Disulfide bonds are covalent linkages between two cysteine residues that typically serve to stabilize protein tertiary structure. The canonical PDI structure across yeast, plants and animals consists of two catalytic thioredoxin domains (a, a') and two non-catalytic domains (b, b') arranged a-b-b'-a' (Kemnick et al 1997).

Thioredoxin domains a and a' have a conserved "CXXC" amino acid sequence, which in classical PDI is "CGHC".

The three-dimensional structure of PDI provides insight into its enzymatic activity. The crystal structure of yeast PDI, characterized by Tian et al. 2006, shows a twisted "U" structure about 80 x 60 Angstroms in size. Catalytic domains a and a' are found on the ends of the "U" shape. Each thioredoxin domain has a central beta-sheet with two alpha-helices on either side. Classical yeast and mammalian PDI also have a C-terminal helix. When the C-terminal domain is truncated, it interacts less with the a' domain, suggesting that an intact C-terminus contributes significantly to PDI activity (Tian et al., 2006). The amino acids comprising and bordering the active sites can adopt different roles depending on their domain (i.e. a or a'). The highly conserved tryptophan residue preceding each active site is suspected to participate in hydrophobic interactions with the substrate. The b and b' domains may contribute to refolding of proteins. The b' domain in particular has a hydrophobic pocket that is capable of binding substrates and occasionally cofactors (Pirneskoski et al. 2004; Russell et al. 2004).

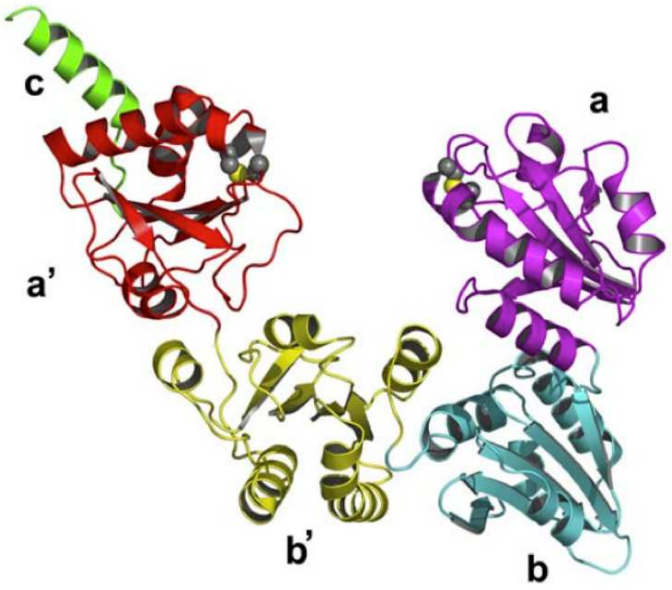

FIGURE 1: The ribbon structure of yeast PDI showing the classical a-b-b'-a' domain arrangement with its C-terminal helix domain. Figure adapted from Tian et al. (2006).

Analysis of the crystal structure of yeast and human PDIs shows a dynamic conformation. In the reduced form of human PDI (hPDI), the a and a' domains are 27.6 A apart. However, oxidized hPDI, i.e. its active sites each have an S-S bond, has a 40.3 A gap between the a and a' domains. The a' domain also twists 45^{o} from its reduced conformation (Wang et al. 2013). The b' domain of the oxidized human PDI is also rotated relative to the yeast structure and reduced human structure. The authors propose that structural dynamism allows hPDI engage in a diversity of isomerase and chaperone activity. It's presently unclear whether the sizeable difference in conformation between reduced and oxidized human PDI is due to its redox status, ligand binding, or a combination of the two (Wang et al. 2013; Freedman et al. 2017).

Furthermore, it is not known whether human PDI changes conformation *in vivo* in response to a changing subcellular redox environment.

Whether PDI oxidizes or reduces a substrate depends on the redox state of its active sites. When folding a newly synthesized protein, PDI's role is typically to create the proper disulfide bond formation. In this case, the substrate would be reduced and PDI's active site oxidized. The bond between PDI's cysteines can be shuffled to the substrate. Then, PDI's active site is reduced and its cysteine unbound, and the nascent protein is folded in its correct conformation. Many PDIs can be oxidatively regenerated by ER oxidoreduction1 (ERO1), which uses oxygen to create a disulfide bond and hydrogen peroxide (Frand and Kaiser 1998; Zito et al. 2010; Tavender et al. 2010). Some oxidizing proteins like Peroxiredoxin4 preferentially oxidize certain PDIs, in this case P5 (Tavender et al. 2010; Sato et al. 2013).

Proteostasis and the Unfolded Protein Response (UPR)

In healthy eukaryotic cells, there is a balance between protein synthesis, folding, export and degradation. Secretory proteins are first translated on ribosomes as part of the rough ER. Their signal peptide directs it to the ER and is cleaved (Blobel 1980). Secretory proteins are folded within the ER lumen, exported to the Golgi and eventually transported to their final destination (Lippincott-Schwartz et al. 2000). Each step is regulated by a finely-tuned network of enzymes and transcription factors that help preserve proteostasis. There are several foldases and chaperones that operate within the ER lumen, including protein disulfide isomerase, whose presence are essential to folding nascent proteins and managing the misfolding of others.

When proteostasis is jeopardized, such that the unfolded proteins accumulate to higher levels than the folding capacity of the ER, ER stress-sensing proteins and transcription factors activate the Unfolded Protein Response (UPR) (Lu and Christopher 2008a). The UPR is a conserved mechanism across eukaryotes that regulates important endoplasmic reticulum chaperones and folding enzymes. The disturbance of ER homeostasis in plants is associated with several growth and developmental defects, including poor seed development, misregulation of programmed cell death (Ondzighi et al. 2008), and light stress (Lu and Christopher 2008b). In mammals, ER stress is the molecular basis for several disease states, as discussed later in this chapter.

There are three main branches of the mammalian UPR: *INOSITOL-REQUIRING ENZYME 1A* (*IRE1α*), *ACTIVATING TRANSCRIPTION FACTOR 6* (*ATF6*), and *PROTEIN KINASE-LIKE ER KINASE* (*PERK*). *Arabidopsis* has homologs to both *IRE1* and *ATF6*, but there is no known *PERK* homolog (Angelos and Brandizzi 2018). IRE1 is a transmembrane protein that serves two critical roles in the UPR. IRE1 has both a cytosolic and ER luminal domain. Its cytosolic side is a kinase and RNase, whereas its luminal side is responsible for sensing ER stress. Calfon et al. (2002) first identified that mammalian IRE1 splices *X-BOX BINDING PROTEIN-1 (XBP1)* as part of the unfolded protein response. XBP1 is a transmembrane protein bound to the ER in non-stressed conditions. When ER stress is sensed, *XBP1* mRNA is spliced by IRE1, producing a transcription factor that regulates parts of the UPR. IRE1 also degrades certain mRNAs on the ER through a process called Regulated IRE1-Dependent Decay (RIDD). RIDD reduces the protein-folding load within the ER by degrading

nascent mRNAs (Hollien and Weissman 2006; Mishiba et al. 2013). *IRE1* has both alpha and beta isoforms in *Arabidopsis* whose functions are thought to overlap substantially.

The *Arabidopsis* transcription factors known for modulating the UPR are bZIP60, bZIP17 and bZIP28. bZIP17 is associated with salinity and osmotic stresses and has mixed expression under chemically-induced ER stress (Henriquez-Valencia et al. 2015; Cifuentes-Esquivel et al. 2018). bZIP28 is a functional homolog of mammalian ATF6. bZIP28 is translocated to the cis-Golgi and processed by *Site-1 protease (S1P)* to its transcription factor form (Liu et al. 2007b; Liu and Howell 2010). *bZIP60* is homologous *to XBP1* and is similarly spliced to its transcription factor form, bZIP60s (Nagashima et al. 2011). *Arabidopsis IRE1a* has a homolog, *IRE1b*, that is apparently also involved in the UPR (Lu and Christopher 2008, Chen and Brandizzi 2012). Recent work found that *IRE1a* and *IRE1b* are both required for proper plant development (Lai et al. 2018).

TABLE 1: Known plant transcription factors and their characteristics

Transcription Factor	**Spliced by**	**Abiotic stress response**	**Mammalian homolog**
bZIP17	SITE-1 Protease (S1P), S2P	Salinity stress (Liu et al. 2007a), Heat stress (Che et al. 2010)	None
bZIP28	S1P, S2P	Heat stress (Gao et al. 2008)	ATF6
bZIP60	IRE1a	Heat stress (Deng et al. 2016)	XBP1

Chemically inducing ER stress is a common method for studying the UPR. ER stress can be chemically induced using dithiothreitol (DTT), a reductant, and tunicamycin (Tm), which

blocks the N-linked glycosylation of secretory proteins leaving the ER (Cox et al. 1993). Previous work done by Lu and Christopher (2008) shows that several PDIs are induced as part of the unfolded protein response along with *Binding Protein 2 (BiP2)* and *bZIP60*. An RNA gel-blot analysis of *AtPDI* gene expressions after 0, 2, and 5 h of tunicamycin treatment showed that *PDI5, PDI6, PDI9, PDI10* and *PDI11* expression increases during ER stress. *BiP2* and *bZIP60* expression also increase under ER stress (Lu and Christopher 2008).

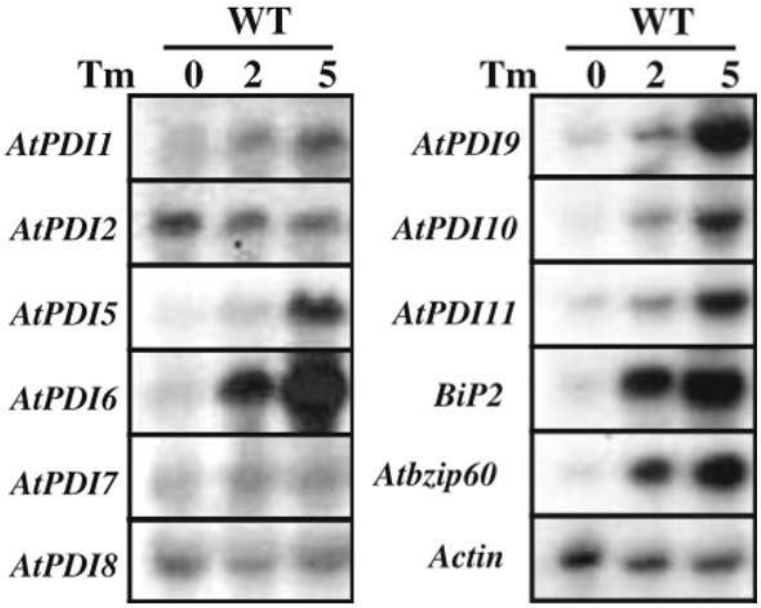

FIGURE 2: RNA blots of AtPDI mRNAs after treatment with tunicamycin (Tm). Figure modified from Lu and Christopher (2008).

The "central dogma" of molecular biology is the immutable progression of DNA to RNA to protein. It is a useful model, but it bears a growing list of profound exceptions. Molecular biology, both in theory and in practice, is increasingly more concerned about systemic and epi-regulation rather than one-directional pathways. Similarly, our understanding of ER stress and

the UPR is being challenged with the advent of new technologies and methods. The central dogma of ER stress is: the accumulation of misfolded proteins, then sensed by ER chaperones, who initiate the UPR by intracellular transcription factors, and alleviate ER stress by the up-regulation of chaperones foldases. Studying the transcriptome of ER stress in stressed and unstressed conditions is an effective approach to gain insight into the pathways but it excludes translational and post-translational regulation. In other words, the current gold standard of studying ER stress via the transcriptome is an effective approach to comparing mutant responses, but it may exclude biologically relevant processes.

The first chaperone implicated in what was not yet called "ER stress" was Glucose Regulated Protein 78 (GRP78). It was initially identified as being highly expressed in glucose-starved tumor cells and eventually as a chaperone that bound improperly folded secretory proteins (Shiu et al. 1977). The "regulation of ER stress proteins" was first described by Lenny and Green (1991) and included two PDIs (*ERp72* and *ERp59*). A year later, the phrase "unfolded protein response" was coined by Gething and Sambrook (1992) to describe the induction of GRP78 in cells overexpressing an influenza protein incapable of properly folding. Binding Protein (BiP) in maize was the first protein in plants to be considered part of the UPR (Fontes et al. 1991). The definition of ER stress was inherently linked to a symptom of protein misfolding, i.e. the induction of chaperones, rather than a direct measurement of misfolded proteins in the ER. Frequently used methods involve comparative mRNA expression of unstressed and stressed samples, measuring the splicing of *XBP1* or *bZIP60* using reporter genes, and quantifying oxidative protein folding via redox-sensitive fluorescent proteins (Lu and Christopher 2008;

Brunsing et al. 2008; Merksamer et al. 2008). Alas, quantifying ER stress separate from the UPR remains a challenge in modern molecular biology.

Despite extensive studies of the UPR in plants, recent findings suggest that the network regulating ER stress response is more complex than previously thought. Howell (2017) explains that, while there is considerable overlap between the UPR and other stress responses, genes induced as part of the UPR should not be assumed to directly mediate protein misfolding. Moreover, Bao et al. (2019) found that the UPR is active in non-stressed conditions and required for vegetative growth. Developmental and whole-plant stressors complicate the single-cell standard of the UPR. For instance, cell-to-cell communication of ER stress is poorly understood. In *Arabidopsis*, spliced bZIP60 can trigger a systemic response by translocating between cells. As an intercellular transcription factor, spliced bZIP60 can induce classic UPR genes in a non-native cell (Lai et al. 2018). Alternatively, the other UPR transcription factors, bZIP17 and bZIP28, are not known to be cell-to-cell mobile. Considering only the two canonical branches of the UPR in plants, there are still gaps in our understanding of their versatility.

Indeed, the genes and transcription factors most associated with the UPR may have distinct, alternative mechanisms to protect cells from stress that are equally important. Hac1, the yeast homolog to bZIP60, is capable of gene repression in addition to its classical role in upregulating agents of the UPR. Van Delfsen et al. (2018) found that the Hac1 transcription factor binds to a distal transcriptional start site (TSS) upstream of the open reading frame (ORF) of proteins distinct from the UPR. The distal TSS produces long undecoded transcript isoforms (LUTIs) that interfere with downstream transcripts. Hac1 not only upregulates proteins to address protein misfolding in the ER, but it down-regulates cellular respiratory proteins

including electron transport chain proteins to reduce the metabolic burden on the cell. The authors speculate that redirecting resources away from respiration during ER stress allows for bolstered lipid metabolism required for cell survival and division. In sum, transcription factor Hac1 has dual responsibilities in regulating the proteome during ER stress. Although transcriptomic studies of ER stress show both up- and down-regulation of genes during the UPR, bZIP60 in plants is only known to up-regulate ER folding machinery.

Functions and phenotypes of protein disulfide isomerase in mammals

The PDI family is ubiquitous in mammalian cells and bears important responsibilities as part of UPR and beyond. Mammals have at least twenty PDI family members, several of which reside within the ER (Bulleid et al. 2011, Sato et al. 2012, Okumura et al. 2015). Mammalian PDIs have been directly implicated in the progression of several diseases, particularly those related to protein misfolding. PDIs are emerging as complex and even duplicitous regulators of cell fate.

There are several examples of PDIs having protective, as well as deleterious, roles in the progression of neurological diseases (for a comprehensive review, see Perri et al. 2016). A prominent example is Alzheimer's disease (AD). Although there are several competing theories for the genesis and progression of AD, most include the accumulation of misfolded proteins in neural cells. The amyloid hypothesis posits that an overproduction of Aβ42, the product of the alternative cleaving of amyloid precursor protein (APP), relative to its clearance is the beginning of a molecular cascade leading to AD. The imbalance of Aβ42 allows for amyloid oligomerization, and eventually amyloid plaques to form in brain tissue (Hardy and Higgins

1992). Aβ42 aggregation is part of a cascade that leads to neuronal cell death, which is associated with the clinical symptoms of dementia, memory loss and personality changes. In cerebral spinal fluid of healthy patients, large amounts of ERp57 was bound to amyloid-beta, suggesting that ERp57 prevents the aggregation of amyloid-beta (Erikson et al. 2005). Additionally, the activation of *PDIA3* and *ERp57* was found to reduce the accumulation of amyloid plaques and neurofibrillary tangles associated with Alzheimer's disease in a mouse model (Tohda et al. 2012). PDI, particularly ERp57, are potential targets in the search for an Alzheimer's disease treatment.

While there is plenty of evidence highlighting the benefits of PDI, several studies indicate PDIs are not exclusively advantageous from a clinical perspective. Literature in the last decade shows increasing evidence for mammalian PDI family members aiding in the progression of several cancers. PDIs may contribute to oncogenesis by facilitating the increased protein folding demand by rapidly growing cancer cells (Lee and Lee 2017). For instance, the human ortholog of PDI14, TNXDC5, has recently been shown to inhibit hypoxia-induced ER stress signaling in cancer cells (Tan et al. 2018). PDI inhibitors are emerging cancer therapies that primarily aim to block oxidative protein folding in cancer cells (Xu et al. 2014).

The IRE1-XBP1 pathway, which PDIA6 has been demonstrated to regulate, has been an intriguing therapeutic target for cancer. Eletto et al. (2014) demonstrates that PDIA6, the mammalian ortholog of PDI9 in plants, is responsible for managing the duration of IRE1 activity. HeLa cells and *C. elegans* lacking *PDIA6* were more sensitive to ER stress inducers such as tunicamycin. Additionally, homozygous *pdia6* knockouts had constitutive UPR. PDIA6 does not primarily limit UPR through improved protein folding in the ER. Instead, PDIA6

controls the inactivation of IRE1 through binding one of one of its three cysteine residues, Cys148. PDIA6 is therefore a direct regulator of IRE1 activity in mammals and is essential for turning "off" the UPR. The potential binding of IRE1 and PDI9 will not be tested in this thesis, but the role of PDI9 in the UPR will be considered in this context.

One study found that spliced *XBP1* is highly expressed in patients with myeloma. Having a lower ratio of spliced to unspliced *XBP1* was correlated with an improved overall survival rate (Bagratuni et al. 2010). Additionally, *XBP1* was found to promote the progression of a human breast cancer subtype (Chen et al. 2014). However, the complexity of the UPR both as a maintainer of proteostasis and as a cell fate regulator has shown mixed results in practice. Kim et al. (2015) describes the IRE1-XBP1 pathway as a "double-edged sword." On the one hand, the intense growth of cancer cells requires an increase in protein folding demands, which may cause ER stress. Inhibiting the cell's ability to relieve ER stress could lead to cell death. That said, the regulatory mechanisms that control ER associated degradation (ERAD) and apoptosis overlap those that maintain proteostasis. In particular, crosstalk between the UPR and ERAD pathways act as both quality- and quantity-control of IRE1 (Hwang and Li 2018). Because IRE1 up-regulates not only UPR genes but also ERAD genes, inhibiting all function of IRE1 may prevent apoptosis or hinder the effect of other therapies. Ultimately, there are still significant gaps in our understanding of how the interplay between the UPR and other cell fate pathways affect cancer proliferation.

Human PDI can have both beneficial and deleterious effects, which brings into question the nature of plant PDI homologs. The role PDI and its homologs are ultimately dependent on cellular context. Yet, studies aiming to characterize plant PDIs generally adopt a positive

hypothesis, such that the PDI of interest benefits cell function. Knockout mutants, therefore, would expect to have reduced function or survival. While no literature on plant PDIs has confirmed a deleterious role in healthy cells, it is plausible that some have multiple, contradictory roles. Our understanding of how PDIs respond to and regulate stress should not exclude the possibility that they are detrimental to growth and development. Given the pathological significance of PDIs in mammals, it's probable that their plant orthologs have important responsibilities yet to be elucidated.

PDI and thioredoxin-like proteins in yeast and E. coli

Single-cell organisms also require disulfide isomerization and make use of thioredoxin family proteins. In *Saccharomyces cerevisiae*, yeast, the *PDI1* gene is essential for viability (Farquhar et al. 1991). PDI1 has two active sites with the canonical "CGHC" amino acid sequence and a "HDEL" putative ER retention signal. As such, it behaves similar to mammalian PDI. There are four PDI-like proteins in yeast that have at least one thioredoxin-like domain: *Eug1p, Mpd1p, Mpd2p,* and *Eps1p*. *Eug1p* has 40% homology to PDI1 and has two thioredoxin-like domains, whereas the other aforementioned homologs have only one thioredoxin-like domain. Interestingly, although *Mpd1p* has only one thioredoxin domain, it is the only yeast PDI-like protein that can fully supplement the loss of *PDI1* (Nørgaard et al. 2001).
In *Escherichia coli* (*E. coli*), there is a family of thioredoxin-like proteins called *dsb.* The active sites of dsb all share the CXXC motif (Aslund and Beckwith 1999). DsbA, for instance, helps form disulfide bonds on newly-synthesized proteins within the periplasm. DsbA is regenerated by DsbB, whose gains its disulfides by reducing quinone (Inaba and Ito 2008). Cho et al. (2011)

demonstrated that *Arabidopsis* PDI2 is capable of restoring disulfide-based protein folding in a *dsbA* mutant. Alkaline phosphatase is a periplasmic enzyme with four disulfide bonds critical for its fnction. Alkaline phosphatase function is reduced in the *dsbA* knockout due to the absence of proper disulfide bond formation. Expressing full-length *PDI2* cDNA in the *dsbA* mutant restored wild-type levels of alkaline phosphatase activity.

Complementation and redundancy of protein disulfide isomerase

The general function of protein disulfide isomerase across species is the same: it is a critical enzyme involved with helping form correct disulfide bonds in proteins. The specific roles, locations and interactions of individual PDI members are still being elucidated. In mammals, PDI family proteins have a wide range of substrates. The original discovery of PDI was in 1963 as an *in vitro* regenerator of ribonuclease, though it was not named "protein disulfide isomerase" until 1975 (Goldberger et al. 1963; Venetianer et al. 1963, Hawkins et al. 1975). Since then, the number of known substrates of mammalian PDI has expanded (Jessop et al. 2009).

That being said, not all PDIs have a breadth of substrates. For instance, venomous marine snails under the *Conus* genus produce cysteine-rich peptides known as conotoxins. Throughout the genus there are an estimated 50,000 different peptides that rely on disulfide bonds for their stability and extracellular function (Bulaj et al. 2003; Bulaj and Olivera 2008). *Conus* have a canonical PDI with two thioredoxin domains which may be regenerated by Ero1 in a manner similar to mammalian PDI (O'Brien et al. 2018). Within the genus, there are five additional identified PDIs that are subjected to higher evolutionary selection than mammalian PDI based on

their variation between *Conus* species (Safavi-Hemami et al. 2016). The diversity of PDIs in the *Conus* genus is proposed to be linked to high positive selection for gene duplications that ultimately increase venom toxicity (Puillandre et al. 2010; Safavi-Hemami et al. 2016). To date, little research has been done into the functional redundancy of the fourteen plant PDIs.

PDIs in plants

Variations on the classical PDI structure found among the fourteen known PDIs in plants can be grouped into six families (Table 2). While previous work has established that several PDIs are part of the UPR, only a handful of plant PDIs have clear physiological phenotypes. The McCormick group found that a truncated *PDI11* mutant (*PDI11Δ*) resulted in disrupted pollen tube guidance, though a full knockout of *PDI11* did not have this effect (Wang et al. 2009). In rice (*Oryza sativa*), the homolog to *PDI9* in *Arabidopsis* is crucial for the formation of seed storage proteins (Onda et al. 2011). *PDI5* is involved in healthy seed development by regulating programmed cell death (PCD) in endothelial cells (Ondzighi et al. 2008). PDI5 has a canonical domain arrangement and is expressed in the endothelial layer of developing seeds. Within the endothelial layer, PDI5 binds cysteine proteases to regulate the timing of PCD and escorts them to protein storage vacuoles. Consequently, a *pdi5Δ* knockout mutant has reduced seed set and embryo viability. The roles and subcellular locations of plant PDIs have proven to be diverse and occasionally unexpected based on their mammalian homologs.

For instance, PDI2 has a unique subcellular localization pattern among *Arabidopsis* PDIs. Although PDI2 is orthologous to mammalian PDI found in the ER, PDI2 was localized with the nucleus and vacuole in addition to the ER (Cho et al. 2011). Using Förster resonance energy

transfer (FRET), PDI2 was found to interact with nuclear protein Maternal Effect Embryo Arrest, MEE8. Subsequent research into the apparent dual trafficking of PDI2 suggests that its interaction with MEE8 results in their post-translational import into the nucleus (Porter et al. 2015). The mechanism for non-secretory localization for other PDIs may be related to competing signals or phosphoylation. For example, *Chlamydomonas reinhardtii* RB60 is a classical PDI which is located in both the ER and chloroplast. Porter et al. (2015) proposes that the phosphorylation of its N-terminal serine and threonine residues may allow transport into the chloroplast, where it then regulates the translation of *psbA* mRNA. Ultimately, canonical plant PDIs are capable of non-canonical locations and interactions.

TABLE 2: *Arabidopsis thaliana* protein disulfide isomerases and their characteristics. Subfamilies are grouped by color with the exception of *PDI8, PDI11*, and *PDI14*, which all belong to separate one-member subfamilies. Adapted from Yuen et al. (2013), Yuen et al. (2017), and Lu and Christopher (2008).

	TAIR code	Domain arrangement	Active sites	Mammalian ortholog	Subcellular location
PDI1	At3g54960	a-b-b'-a'	CGAC; CHCH	PDI, PDIp, PDILT, ERp57	ER
PDI2	At5g60640	a-b-b'-a'	CGHC; CGHC	PDI, PDIp, PDILT, ERp57	ER
PDI3	At1g52260	a-b-b'-a'	CARS; CVNC	PDI, PDIp, PDILT, ERp57	ER
PDI4	At3g16110	a-b-b'-a'	CARS; CINC	PDI, PDIp, PDILT, ERp57	ER
PDI5	At1g21750	a-b-b'-a'	CGHC; CGHC	PDI, PDIp, PDILT, ERp57	ER
PDI6	At1g77510	a-b-b'-a'	CGHC; CGHC	PDI, PDIp, PDILT, ERp57	ER
PDI7	At4g27080	a-COPII	CYWC	Erv41p/Erv46p	ER and cis-Golgi
PDI8	At1g35620	a-b-b'	CGHC	HsTMX3	ER and Golgi (unpublished)
PDI9	At2g32920	a^o-a-b	CGHC; CGHC	P5, HsPDIA6	ER with punctate structures
PDI10	At1g04980	a^o-a-b	CGHC; CGHC	P5, HsPDIA6	ER with punctate structures
PDI11	At2g47470	a-a'-D	CGHC-CGHC	N/A	ER
PDI12	At3g20560	a-COPII	CYWS	Erv41p/Erv46p	Unknown
PDI13	At1g50950	a-COPII	CYWS	Erv41p/Erv46p	Unknown
PDI14	At1g07960	a	CKHC	TXNDC5	Unknown

PDI9, the central protein of investigation for this thesis, falls under the PDI-M family, whose domain arrangement is a^{o}-a-b. Each of its catalytic domains contains a "CGHC" motif. *PDI9* may also be referred to in literature as *AtPDI9* or *PDIL2-3*; its TAIR code is At2g32920 (Yuen et al. 2013). PDI10 is a homolog within the same subfamily as PDI9, though it has an ER retention signal "KDDL" rather than "KDEL".

Previous work in the Christopher Laboratory has shown that PDI9 is located within the ER lumen (Yuen et al. 2013). Figure 3 shows that PDI9 and its homolog PDI10 both co-localize with the ER. Interestingly, they form distinct punctate structures. Subsequent work has attempted to determine what these punctate are, whether storage protein bodies, specialized vacuoles, or aggregated PDI9 within the ER lumen (Yuen et al. 2013; unpublished data). However, it remains unclear under which environmental conditions and developmental stages these PDI9 and PDI10 punctate are found.

Unpublished work by Smith (2015) shown in Figure 4 suggests that *PDI9* is highly expressed in floral tissues. The *PDI9* promoter was fused to the beta-glucuronidase gene from *E. coli* and transformed into wild-type (Col-0) *Arabidopsis thaliana.* When exposed to the X-gluc substrate (5-bromo-4-chloro-3-indolyl glucuronide), the beta-glucuronidase enzyme creates a blue compound, thereby showing the activity of the *PDI9* promoter. Pro_{PDI9}:GUS activity is high in mature anthers and dehisced pollen.

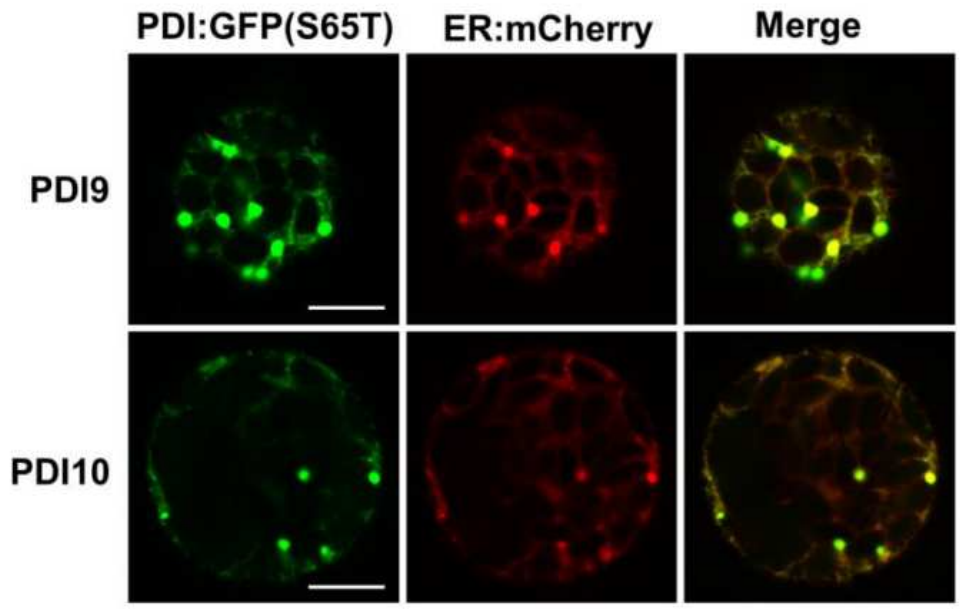

FIGURE 3: Transfected mesophyll protoplasts show *PDI9* and *PDI10* co-localize with the ER and form punctate structures**.** Scale bar is 10 um. Figure from Yuen et al. (2013).

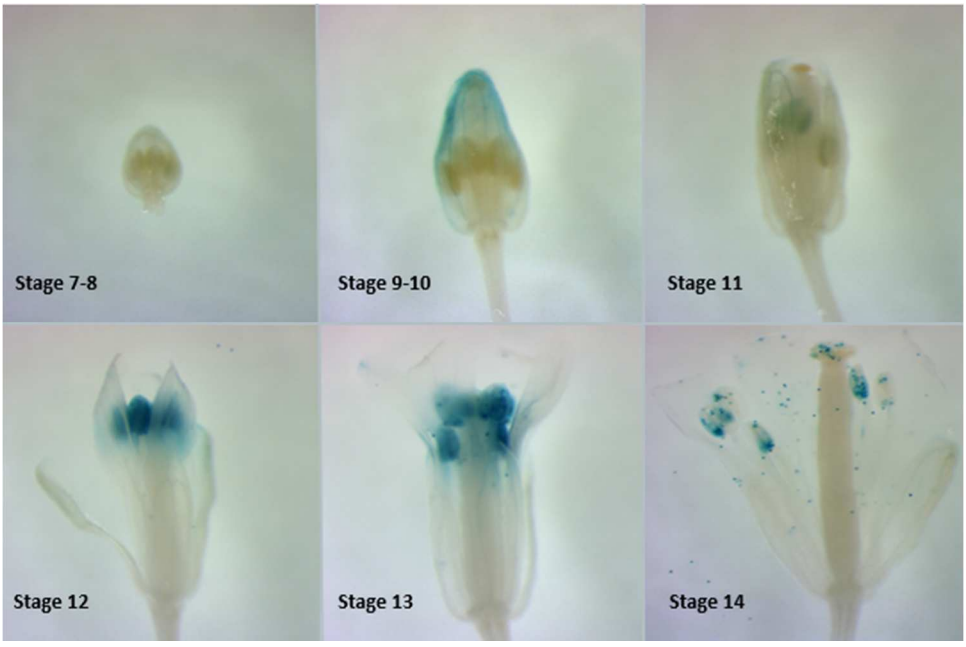

FIGURE 4: Pro$_{PDI9}$:GUS fusion shows *PDI9* is highly expressed in mature anthers and pollen. Figure from Tyler Smith (2015, unpublished).

These preliminary data show that PDI9 localizes in the ER, folds proteins via disulfide bonds (Yuen et al. 2013) and is highly expressed in developing and mature pollen. Additionally, Lu and Christopher (2008) demonstrate that *PDI9* is induced as part of the *Arabidopsis* UPR, along with several other *PDI*s and chaperone *BiP2*. Subsequent studies of *bZIP17/bZIP28* plants have 150% higher expression of *PDI9* than wild-type, whereas *17/60, 28/60* and *60* alone mutants have a diminished response of *PDI9* to ER stress (Kim et al. 2018).

Plant reproduction and proteostasis

Plants have an alternating life cycle, with diploid sporophyte and haploid gametophyte stages. In *Arabidopsis*, pollen is the male gametophyte and the embryo sac is the female gametophyte. Mature pollen is tricellular: two sperm cells are enclosed by a larger cell (reference). A single mature pollen grain is on average 23 microns long, 13 microns wide, and shaped a bit like a football. Pollen development occurs within anthers. Each *Arabidopsis* flower has four anthers with stamens that extend close to the stigma, and two shorter anthers. Unstressed wild-type flowers can produce thousands of viable pollen grains (reference). *Arabidopsis* has perfect flowers that almost exclusively self-pollinate.

The tapetum is a tissue within anthers that surrounds maturing pollen. It is critical for coordinating processes that comprise its viability (Goldberg et al. 1993; Zhu et al. 2011). When pollen grains reach maturity, pollen release from anthers is made possible by the programmed cell death of the tapetum (Kawanabe et al. 2006). Delays or disruption in tapetum function can ultimately lead to male sterility. The anther environment, particularly the tapetum, lays the foundation for healthy, viable pollen grains.

The development of the mature pollen cell wall begins within the tapetum. The cell wall is important throughout sexual reproduction: it provides a physical barrier protecting sperm cells from abiotic stress, mediates pollen-stigma adhesion via its lipophilic composition, and is critical for pollen hydration prior to forming a pollen tube (Pacini et al. 1985; Ariizumi and Toriyama 2011; Zinkl et al. 1999). The composition of the pollen cell wall changes throughout development. Callose, for example, is a β-1,3-glucan polymer that surround microspores and tetrad pollen. During the transition from tetrad to uninucleate microspores, the callose cell wall is enzymatically digested (Verma and Hong 2001). Callose is not present in mature pollen grains, but it is found downstream as callose plugs in pollen tubes (Nishikawa et al. 2005). The production and dissolution of cell wall components is precisely regulated by a transcription factor cascade (Xu et al. 2014; Li et al. 2017).

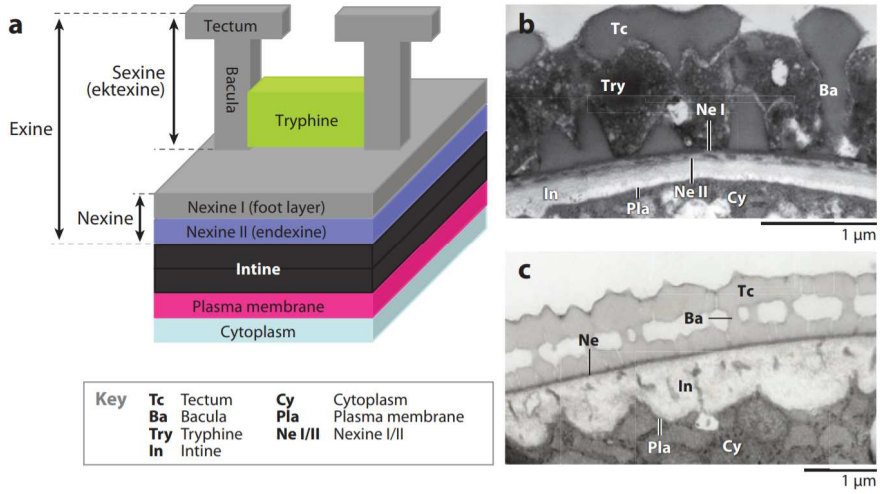

FIGURE 5: Angiosperm pollen cell wall structure. A typical angiosperm pollen grain (a) and transmission electron micrographs of a cross-section of exine architecture in Arabidopsis (b) and mature rice (c) pollen grains. Figure from Ariizumi and Toriyama (2011).

The outer cell has two layers of cell wall, the intine and the exine (Figure 5). The intine is thought to be a mixture of pectin and cellulose but a direct measurement of intine composition has not been done as of writing (Heslop-Harrison 1968; Radja et al. 2019). The primary component of the exine layer is an evolutionarily-conserved heterogeneous compound known as sporopollenin. Sporopollenin gives pollen its incredible resistance to desiccation and degradation. Tapetum plastids are responsible for the *de novo* synthesis of fatty acids and polyketides, which are modified in the tapetum ER before extracellular export as sporopollenin monomers to the pollen grain (Ahlers et al. 1999; Quilichini et al. 2015; Battat et al. 2019). *Arabidopsis thaliana* pollen exine are complex and reticulated, but other species like *Oryza sativa* have a smooth exine (Ariizumi and Toriyama 2011). Differences in the reproduction cycle, including wind pollination and help from pollinator species, are thought to influence the evolution of pollen cell diversity.

Male reproductive development is particularly sensitive to heat stress. Heat stress has several impacts of male reproductive development in plant species, including disrupted anther dehiscence, shorter anthers, and the disruption of male meiosis (Sato et al. 2006; Sakata et al. 2010; Endo et al. 2009). Additionally, heat stress can reduce pollen fertility by stunting pollen production, maturation, and pollen tube growth (Barnabas et al. 2008; Zinn et al. 2006). Temperatures as low as 27^{o}C have tangible detrimental effects on survival (Ludwig-Muller et al 2000). There is ample physiological evidence that heat stress negatively impacts plant reproduction, both in the laboratory and in agricultural fields.

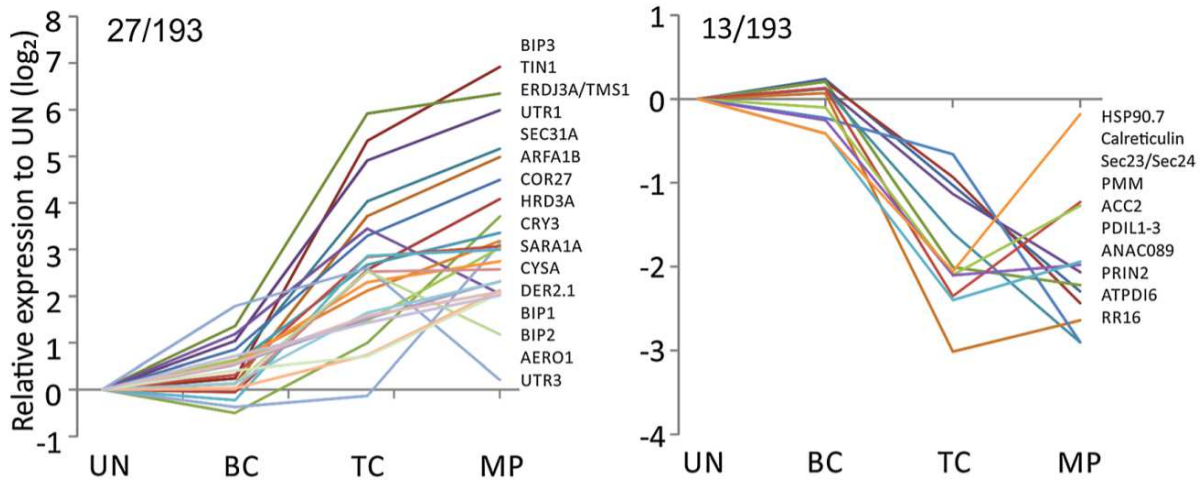

FIGURE 6: Expression of UPR-related genes during pollen development and germination. Arabidopsis thaliana genes showing differential expression (log2) of >twofold or <-twofold during male gametophyte development from unicellular to tricellular pollen. UN unicellular, BC bicellular, TC tricellular, DP dry pollen. Figure from Fragkostefanakis (2016) using transcriptomic data from Honys and Twell (2004).

On a molecular level, heat stress and the unfolded protein response are closely linked. Pollen development places a high demand on protein synthesis and folding even under healthy conditions made evident by up-regulation of UPR enzymes (Honys and Twell 2003; Iwata et al. 2008). For instance, floral tissues have low levels of spliced bZIP60 in non-stressed conditions (Deng et al. 2013). Figure 6 shows the relative expression of UPR genes during pollen development. Certain PDIs are up-regulated as pollen matures while others are down-regulated. For instance, *PDI5* expression decreases from unicellular pollen to mature pollen. *PDI6* expression decreases between unicellular and tricellular pollen but rebounds in mature pollen grains. The expression of *PDI9* and *PDI10* is fairly constant throughout pollen development.

Mutants of several UPR genes have disrupted male gametophyte development. Pollen tube growth is stunted in a *bip1-bip2* knockout mutant in non-stressed conditions (Maruyama et al 2014). *THERMOSENSITIVE MALE STERILE 1 (TMS1)* encodes a heat shock-like protein with a PDI domain that is expressed in pollen tubes. Knockout mutants had morphologically normal pollen grains at 30ºC heat stress but significantly retarded pollen tube growth (Yang et al. 2009). An *ire1a/ire1b* knockout has severely deformed pollen coats under only 27.5ºC heat stress (Deng et al. 2016). In summary, proteins involved in the UPR are upregulated in pollen development and putatively critical for proper development under heat stress.

PDI9 and its potential interactors

Yeast two-hybrid screening is a tool for identifying protein-protein interactors. The primary protein of interest acts as the "bait" and millions of potential interactors are the "prey". The transcription factor for a reporter gene is split into two fragments: one that binds the DNA upstream of the reporter gene, and another fragment that activates transcription. Both fragments are normally required to be in close proximity for transcription of the reporter gene. The DNA-binding fragment is attached to the bait protein and prey proteins are attached to the activating fragment. Only when the bait binds the prey will transcription of the reporter gene occur. Thus, proteins that interact with the bait protein can be identified by reporter gene activity. *PDI9* was used as the bait protein for a yeast two-hybrid screening done in 2004 by Molecular Interaction Facility.

FIGURE 7: Domain arrangements of two potential PDI9 interactors. LRX8 (top) and EMC7 (bottom)**.** sp signal peptide, LRR leucine rich repeat domain, Cys cysteine-rich domain, EXT extensin domain, DUF domain of unknown function 2012, t transmembrane domain.

One of the putative interactors of PDI9 from yeast two-hybrid screening is a leucine rich repeat-extensin chimera (LRX) family protein. *LRX8* (TAIR code AT3G19020), also referred to as *PEX1*, encodes a structural component of cell walls (Baumberger et al. 2003; Borassi et al. 2015). LRX8 has a signal peptide (amino acids 1-30) as predicted by SignalP 5.0 (score: 0.24). The N-terminal half of LRX8 contains a leucine-rich repeat (LRR) domain (amino acids 39-332) as well as a cysteine-rich domain (amino acids 352-397) (Baumberger et al. 2003). The C-terminal half contains a highly-repetitive extensin domain (amino acids 408-956). The repeated motif "PPPVXS" found in LRX8 is characteristic of hydroxyproline-rich glycoprotein extensin (Baumberger et al. 2001, Lamport et al. 2011; Zhang et al. 2008). The N-terminal LRR domain is thought to be involved in protein-protein interactions and the C-terminal anchors the protein within the cell wall (Baumberger et al. 2003; Ringli 2010). There are four *LRX* genes that are highly expressed in mature pollen and pollen tubes, *LRX8-11* (Rigli 2005). In general, the LRX family proteins are responsible for the proper assembly of cell walls.

LRX proteins have recently gained notice for their role in pollen cell walls. Pollen tubes must maintain a fine balance of turgidity and softness to allow for growth and structural

integrity. Knockout mutations of pollen-expressed *LRX* genes result in a dramatic reduction in pollen germination and pollen tube growth. The cell wall of double mutants is less dense, causing pollen tube growth to be "wavy" with bulging cell walls (Sede et al. 2018; Fabrice et al. 2018). Importantly, Alexander viability staining of anthers shows no substantive difference in pollen viability between wild-type and *LRX* double and triple knockout mutants, thus their impact on cell wall organization putatively begins at pollen germination. The pollen LRX proteins also control pollen tube growth by binding secreted peptides called RAPID ALKALINIZATION FACTORs (RALFs). RALF4 binds LRX8 and LRX9 to stop pollen tube growth. The authors propose that the LRX8/9-RALF4 interaction helps the pollen tube sense the extracellular female tissues on its path to fertilization (Mecchia et al. 2017). Triple and quadruple knockout mutants have shorter siliques with reduced seed set (Figure 8; Wang et al. 2017). These findings indicate pollen LRX proteins play important, overlapping roles in ensuring the assembly of cell walls in growing pollen tubes with implications on seed set.

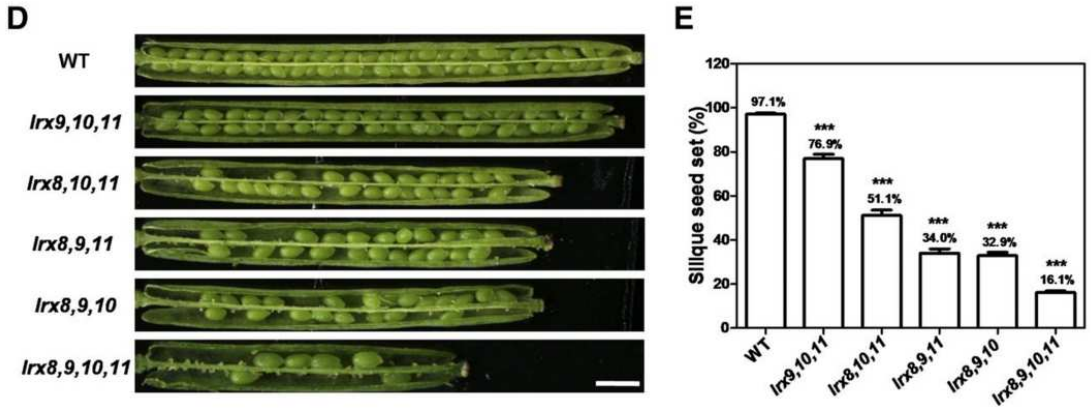

FIGURE 8: Triple and quadruple knockout mutants of the pollen *LRX* family members (*LRX8-11*) have significantly reduced seed set. Figure from Wang et al (2017).

Leucine-rich repeat domains are widespread in eukaryotes and have the common task of mediating protein-protein interactions (Kobe and Deisenhofer 1994; Forsthoefel et al. 2010). Plant intracellular Ras-group-related leucine rich repeat proteins, or PIRLs, are a small family of plant-specific proteins with an LRR domain (Forsthoefel et al. 2005). PIRL1 and PIRL9 are essential for early pollen development. *pirl1-pirl9* double KO pollen grains are less viable, exhibit arrested growth, and fail to produce a callose wall (Forsthoefel et al. 2010). A broader lens of LRR domain-containing proteins suggests that the LRR domain of *LRX8* may influence pollen cell wall development independent of its extensin domain.

The other protein identified from the yeast two-hybrid screen is ER Membrane Complex Subunit 7 (EMC7; TAIR code AT4G32130). EMC7 is a relatively small 22 kDa protein with no cysteines and has 53% similarity to human EMC7. EMC7 has a signal peptide (amino acids 1-29) as predicted by SignalP 5.0 (score: 0.80) and a domain of unknown function (DUF 2012) (amino acids 52-156). *EMC7* is expressed in mature pollen and is possibly associated with the Golgi apparatus based on its appearance in a transcriptomics study, though this somewhat conflicts with the mammalian homolog's subcellular location (Nikolovski et al. 2012). As of writing, there is no literature describing the function of any EMC subunits in *Arabidopsis thaliana.*

The EMC is conserved among eukaryotes; yeast EMC has six subunits, whereas human EMC has ten subunits. Only two of the subunits are paralogous; eight of the 10 subunits are transmembrane proteins (Wideman 2015). Loss of mammalian EMC results in ER stress. Jonikas et al. (2009) was the first to identify and name "EMC" in yeast. They measured the expression of GFP linked to a *Hac1p* promoter- Hac1p is orthologous to spliced bZIP60 in *Arabidopsis*- with

increasing doses of DTT in thousands of *Saccharomyces cerevisiae* mutants. Six mutants, named *EMC1* through *EMC6*, had a significant increase in the expression of Pro_{Hac1p}:GFP. Yeast *EMC1* through *EMC6* strongly alleviated the deletion of each other and had a stoichiometric relationship to another. Mutant yeast strains without these six EMC proteins have an accumulation of misfolded membrane proteins (Jonikas et al. 2009).

Mammalian EMC has been implicated in ERAD. Recent literature has shown that mammalian EMC aids in the synthesis and folding of multipass transmembrane proteins. The six core EMC proteins, EMC1 through EMC6, cooperate with heat shock proteins, BiP and membrane protein-specific chaperones to aid in the translation of transmembrane proteins (Shurtleff et al. 2018). The EMC core also associates with ribosomal proteins, suggesting that EMC acts nearly contemporaneously with TMD synthesis, rather than downstream. Shurtleff et al. (2018) found that EMC has a preference for TMDs with charged residues and relatively less dominant hydrophobic residues.

Furthermore, mammalian EMC is required for the proper topogenesis of many transmembrane proteins. Chitwood et al. (2018) found that EMC is required for correctly orienting β1-adrenergic receptor (β1AR), a G-protein-coupled receptor (GPCR), via its first TMD. The same group also found that EMC is required for the insertion of many moderately hydrophobic transmembrane proteins. They attribute its association to ER stress as a secondary effect rather than a direct mediator, in that protein mislocation due to a disruption of EMC activity results in ER stress and not EMC mediating ER stress in a manner similar to PDIs or BiP (Guna et al. 2018). However, other studies directly link the EMC to ER stress. Silencing of *EMC1, EMC2, EMC3, EMC4,* and *EMC6* individually in *Caenorhabditis elegans* (*C. elegans)*

using RNAi resulted in ER stress as measured by GFP under heat shock protein-4 (hsp4) promoter (Richard et al. 2013). Whether *Arabidopsis EMC7* behaves in a similar manner is yet to be determined.

CHAPTER II: RATIONALE, HYPOTHESES, AND OBJECTIVES

Significance of work

Basic and applied plant sciences are cornerstones to current and future food security. Global warming is expected to increase the frequency and severity of weather events in addition to raising average mean temperature. Impending temperature increases are predicted to more negatively impact yields of tropical field crops than those in mid- to high-elevation agricultural zones (Rosenzweig et al. 2013). Unpredictable weather affects farmers, commodity prices and the food supply. Compounding the issue is population growth, which is expected to reach 9.7 billion people in only thirty years' time (United Nations 2017). Conservative estimates state that we need to increase our food supply by 70% to meet rising demands, climate change notwithstanding. Feeding the world is a daunting challenge, one which many experts believe has no single solution.

Genetic engineering of food crops is a plausible adaptation to many climate change impacts. Maruyama et al. (2016) used bioinformatic tools to create a novel heat shock response element (HSE) promoter to improve abiotic stress tolerance in soybean, rice, and maize. Most recently, Eisenhut and Weber (2019) used tobacco to improve photosynthetic efficiency by eliminating the creation of a RuBisCO byproduct, thereby increasing potential yield. A non-classical PDI from *Methanothermobacter thermautotrophicus*, a thermophilic archaeon, conferred heat stress tolerance when transformed into rice (Wang et al. 2018). Transgenic *MtPDI* rice plants had an improved survival rate under an acute (24 h) 42^{o}C heat stress. Breeding for

abiotic stress tolerance and yield are two major goals of seed companies. Novel transgenic approaches like those above, albeit untested on a commercial basis, have promise.

Plant fertility is directly linked to seed and fruit production. Heat stress during flowering has a well-documented detrimental effect on yields of major food crops like maize (Gourdji et al. 2013), soybean (Djanaguiraman et al. 2013), rice and wheat (Barnabas et al. 2008). While the physiological impacts of heat stress are clear, the molecular underpinnings are not. There is a need for more research on the impact of prolonged heat stress. Studies of heat stress in *Arabidopsis* are frequently only focused on acute heat stress and may exclude important, real-world environmental conditions. Prolonged heat stress, like prolonged ER stress, can lead to molecular adaptations. As mentioned above, mammalian *IRE1* and *PDI* have complex responsibilities during the UPR that make therapeutics difficult. Cellular processes are almost never black-and-white and the functions of *PDI* are no exception. *PDI9* and *PDI10* are known agents of the plant UPR but their specific roles are yet to be determined. Studying their impacts on pollen viability during heat stress could provide a novel perspective describing the context-dependent behaviors of PDIs in the UPR. Moreover, studying the PDI-M subfamily gives insight into the molecular response to abiotic stress. Because of the high expression of *PDI9* in pollen, understanding the role of *PDI9* could inform molecular approaches to improving pollen viability and germination. Downstream application of our improved understanding of *PDI9*'s role in pollen viability could lead to agricultural crops with increased resilience under heat stress.

Research questions and hypotheses

The objective of this master's thesis is to characterize the role of *PDI9* in pollen biogenesis in *Arabidopsis thaliana.* Specifically, I aim to document the physiological and molecular impacts of *PDI9* on pollen development during heat stress.

PDI9 and *PDI10* genomic DNA sequences have 79% identity; they each share the a-a'-b domain arrangement. Furthermore, previous work by Lu and Christopher (2008) demonstrated that both *PDI9* and *PDI10* are up-regulated in response to induced ER stress. Notably, PDI9 has a canonical "KDEL" ER retention signal, whereas PDI10 has "KDDL". First, I hypothesize that *PDI9* and its homolog *PDI10* have similar but not identical responsibilities in pollen biogenesis.

Recent literature on mammalian and yeast EMC suggest that EMC is involved in ER-associated degradation (ERAD). The UPR and ERAD have different means of restoring cellular homeostasis, but the proteins involved are not mutually exclusive. Though there is virtually no research on plant EMC, I hope to lay the foundation for studying plant EMC by exploring the link between *PDI9*, a well-established agent of the UPR, and *EMC7*. I hypothesize that EMC7 is a membrane protein that is at least partially associated within the ER. Additionally, I hypothesize that PDI9 interacts with EMC7, possibly through crosstalk of the UPR and ERAD pathways.

LRX8 has a signal peptide, so I expect it to pass through the secretory pathway before fulfilling its role as a cell wall protein. I hypothesize that PDI9 also interacts with LRX8 as it moves through the secretory pathway. The N-terminal half of LRX8 has thirteen cysteine residues, whereas the C-terminal extensin domain has none. The positions of these cysteines are conserved among the LRX subfamily, indicating that disulfide bonds are critical to the final conformation or function of LRXs. Therefore, it seems most likely that PDI9 interacts with the

N-terminal half of LRX8. Furthermore, because LRX8 is a pollen cell wall protein, I hypothesize that *pdi9* knockout plants will have pollen cell wall defects.

Thorough genetic analysis is required to determine the contribution of *PDI9* and *PDI10* each in pollen biogenesis. The *pdi9* and *pdi10* single knockouts will provide insight into whether or not the pollen phenotype is caused by one or both genes. The absence of one PDI-M subfamily member may not in itself cause ER stress if the other member is present, thus the *pdi9-pdi10* double knockout will be used to evaluate the phenotype in the absence of both PDI-M subfamily members.

Finally, I hypothesize that *PDI9* plays a role in pollen development during heat stress that manifests with both a molecular and physiological phenotype. First, Pro_{PDI9}:GUS staining done by Smith (2015) demonstrated that *PDI9* is highly expressed in developing anthers and mature pollen. Second, PDI9 is an ER resident protein with a known response during ER stress. Third, heat stress has detrimental effects on pollen development whose cause is partially ER stress. Therefore, investigating the function of *PDI9* as an agent of the UPR response in developing pollen is the subject of this thesis. I hypothesize that the *pdi9* single KO and the *pdi9-pdi10* double KO will be more sensitive to heat stress. A PDI9 antiserum and a *PDI9* over-expressor line are available for protein and genetic analyses. Using the methods outlined in this thesis, I aim to define the *PDI9* heat stress phenotype and its protein-protein interactions that mediate the development of healthy pollen.

Objectives

1. Demonstrate the co-localization of PDI9 with potential protein interactors EMC7 and LRX8 in transfected protoplasts
    a. Confirm the subcellular location of EMC7 by demonstrating co-localization with ER and Golgi body markers
    b. Confirm that LRX8 passes through the secretory pathway via localization in the ER, therefore demonstrating proximity to PDI9.
2. Authenticate the genotypes of previously created *PDI9* and *PDI10* mutants and characterize their expression of related UPR genes
    a. Isolate DNA and RNA from *pdi9* and *pdi10* single knockout mutants, *pdi9-pdi10* double knockout mutants, and *35S:PDI9* overexpressor. Synthesize first strand cDNA from RNA.
    b. Use PCR and RT-PCR to verify the presence and expression, respectively, of the expected genes and/or T-DNA insertions
    c. Isolate protein from key tissues of each genotype mentioned above. Use Western blot analysis with a PDI9-specific antiserum and Coomassie staining to confirm the presence or absence of PDI9 and PDI10 proteins
    d. Characterize the difference in expression between wild-type and *pdi9-pdi10* KO seedlings under induced ER stress by quantitative real-time PCR (qPCR)

3. Identify and characterize the physiological effect of *PDI9* on pollen biogenesis and plant reproduction
    a. Confirm the presence of PDI9 in floral tissues
        i. Isolate proteins from pollen, anthers, and whole flowers from wild-type and PDI9 mutants
        ii. Compare protein expression between genotypes and tissues via Western blotting with PDI9 antiserum
    b. Assess percent viability and total pollen grain counts of each genotype under non-stressed and heat-stressed conditions using modified Alexander viability staining
        i. Develop efficient method for isolating and assessing pollen viability and number of dehisced pollen grains using modified Alexander staining
    c. Use scanning electron microscopy (SEM) to identify morphological differences between non-stressed and heat-stressed pollen for all genotypes
    d. Quantify the potential impact of *PDI9*'s role on silique length under heat stress

CHAPTER III: CO-LOCALIZATION OF PROTEINS IN TRANSFECTED PROTOPLASTS

Introduction

Protein-protein interactions can be assessed qualitatively and quantitatively through co-localization experiments. Essentially, proteins of interest are fused to unique reporter genes and their overlapping signals are an indication that they occupy the same subcellular location. Transient expression in protoplasts, cells with their cell wall removed by digestion, is a time-efficient approach to visually assessing a protein's location (Wu et al. 2009, Yuen et al. 2013). One, two, or several plasmids can be expressed by a single transfected protoplast, allowing for multiple reporter genes to be used at once. Analysis can be either qualitative, wherein several images of protoplasts are used to categorize a protein's subcellular location, or quantitative. Percent merged fluorescence and fluorescence resonance energy transfer (FRET) are common techniques used to quantitatively assess a protein's location in proximity to others.

Here, co-localization experiments in plant protoplasts were used to assess the subcellular locations of PDI9 with LRX8 and EMC7. PDI9 is a well-established ER-resident protein, as discussed in Chapter I. In the case of LRX8, a chimeric leucine-rich repeat and extensin protein, the protein's final destination is known to be the cell wall. Because LRX8 has a signal peptide, I predicted that it would show some co-localization with the ER as it moves along the secretory pathway. Based on the location of its homologs in other species, EMC7 is plausibly a transmembrane protein bound to the ER. However, there is no prior literature confirming the subcellular location of *Arabidopsis thaliana* EMC7.

Methods

Construct design and plasmid subcloning

First, constructs were made for *LRX8* and *EMC7*. The design is shown below in Figure 9. The constitutive promoter 35S, mCherry fluorescent protein, and NOS terminator were ligated to the pBluescript ks+ vector. Both genes of interest were ligated between the XhoI and NdeI restriction sites. Translational fusions of LRX8 or EMC7 with mCherry make it possible to measure protein location in relation to the previously created PDI9:eGFP:KDEL fluorescent translational fusion (Yuen et al. 2013).

FIGURE 9: Plasmid design for co-localization experiments showing the restriction sites used on pBluescript ks+ and the gene of interest (*LRX8*, *EMC7*).

Full length *EMC7* was amplified from cDNA clone U17125 from TAIR. Forward primer sequence: 5' TTTTCTCGAGATGGCGCCGATTTTCAGATCCACTTC 3'. Reverse primer sequence: 5' TTTCATATGGCGGCTAGCGGGTAACAAGCTAG 3'. PCR reaction for *EMC7* was as follows: 32.5 uL ddH_2O, 10 uL 5X Phusion buffer, 1 uL 10 mM dNTPs, 2.5 uL 10 uM forward primer, 2.5 uL 10 uM reverse primer, 1 uL cDNA, 0.5 uL Phusion enzyme. PCR conditions were as follows: 98^{o}C 2 minutes; 98^{o}C 15 seconds, 61^{o}C 30 seconds, 72^{o}C 3 minutes

for 30 cycles; 72ºC 10 minutes. The resulting fragment is 609 base pairs, with XhoI and NdeI restriction sites on the 5' and 3' ends, respectively.

There were several unsuccessful attempts at expressing *LRX8* in protoplasts using a variety of amplicons. To improve expression, full length *LRX8* with 21 base pairs of its 5' UTR was eventually amplified from wild-type (Col-0 ecotype) genomic DNA. Forward primer sequence: 5' TTTCTCGAGTTTCCAAGTTTTTCCATCACC 3'. Reverse primer sequence: 5' AAAACATATGGTAGCCTGGGAACATCGGTGG 3'. PCR reaction for *LRX8* (with 5' UTR) was as follows: 26.5 uL ddH_2O, 6 uL 25% DMSO, 10 uL 5X Phusion buffer, 1 uL 10 mM dNTPs, 2.5 uL 10 uM forward primer, 2.5 uL 10 uM reverse primer, 1 uL genomic DNA, 0.5 uL Phusion enzyme. PCR conditions were as follows: 98ºC 2 minutes; 98ºC 15 seconds, 63ºC 30 seconds, 72ºC 3:30 minutes for 35 cycles; 72ºC 10 minutes. The resulting fragment is 2898 base pairs, with XhoI and NdeI restriction sites on the 5' and 3' ends, respectively.

The 35S promoter was amplified from pCambia1302 plasmid. Forward primer for 35S: 5' TCAGGGTACCTTCATGGAGTCAAAGATTC 3'. Reverse primer: 5' ATCTACTCGAGTCAAGAGTCCCCCGTG 3'. mCherry and NOS terminator were amplified together from plasmid pBL[35S:Man49-mCherry] described (Yuen et al. 2017) . Forward primer: 5' CACCGACTAGTCATATGGTGAGCAAGGGCGAGGA 3'. Reverse primer: 5' TAGTTGAGCTCCCGATCTAGTAACATAGA 3'. PCR reaction was the same as the reaction for *EMC7*. PCR conditions were as follows: 98ºC 2 minutes; 98ºC 15 seconds, 60ºC 30 seconds, 72ºC 1 minute for 30 cycles; 72ºC 10 minutes. The 35S promoter and the mCherry:NOS terminator amplicons were 545 and 962 base pairs, respectively. 35S promoter has KpnI

restriction site on its 5' end and XhoI on its 3' end. mCherry:NOS has NdeI on its 5' end and SacI on its 3' end.

PCR products were separated using electrophoresis and purified after excising from agarose gel. Purified amplicons were digested as follows: 15 uL purified amplicon, 10 uL ddH_2O, 3 uL 10X CutSmart buffer, 1 uL 5' enzyme, 1 uL 3' enzyme. Digestion reactions were placed in a 37 ^oC bath for at least one hour. The digestion was separated using electrophoresis. The digested amplicon was excised from agarose gel and purified.

Digested fragments were ligated in the following order: 35S promoter to pBluescript ks+ backbone, mCherry to 35S:pBluescript, 35S:mCherry to the gene of interest. Ligation reaction: 10 uL digested fragment, 5 uL digested plasmid, 2 uL 10 mM rATP, 2 uL 10 T4 ligase buffer, 1 uL T4 ligase. Reaction occurred at 16 ^oC for at least one hour or room temperature (about 22 ^oC) for 15 minutes.

Ligated products were transformed into competent *E. coli* cells (DH5α strain). 3 uL of ligation reaction was added to 30 uL thawed competent cells. After growing at 37 ^oC at 225 rpm for 42 minutes, cells were spread on LB plates with 100 ug/mL carbenicillin. Plates were incubated at 37 ^oC overnight. Single colonies were added to 5 mL LB and incubated for 14 h at 37 ^oC and 225 rpm. Plasmid DNA was isolated from cultures using Machery-Nagel plasmid prep kit. Plasmid DNA was sent to Genewiz for Sanger sequencing to verify correct sequence and translational frame. Sequenced plasmids were made endotoxin-free using the Machery-Nagel maxi prep kit.

Organelle markers were characterized by the Nebenführ Laboratory and modified for use in protoplasts. The Golgi marker "G-gk" was digested from its pBIN binary vector backbone and

ligated into the pBluescript ks+ backbone. Their marker uses soybean mannosidase with GFP at the C-terminus. ER marker "ER-rk" uses the signal peptide of Arabidopsis thaliana wall-associated kinase 2 (AtWAK2) at the N-terminus of mCherry and an HDEL ER retention signal at the C-terminus. Both constructs use a double 35S promoter (Nelson et al. 2007).

Protoplast transfection and laser scanning confocal microscopy

Mesophyll protoplasts from 3 to 4-week-old *Arabidopsis* rosette leaves grown in 16 h light/8 h dark at 22 ºC were transfected by the Tape-Arabidopsis sandwich method as described (Wu et al. 2009). 30 ug total plasmid DNA was transfected per sample, with approximately 15 ug each plasmid. Cells were viewed with the Olympus Fluoview 1000 laser scanning confocal microscope or the Leica TCS SP8 X with white light laser scanning confocal microscope at the Biological Electron Microscopy Facility at UH Mānoa. Images were processed using ImageJ. Any adjustments to brightness, contrast or gamma were applied to the entire image to avoid bias or artifacts.

Results

EMC7 and PDI9 co-localization

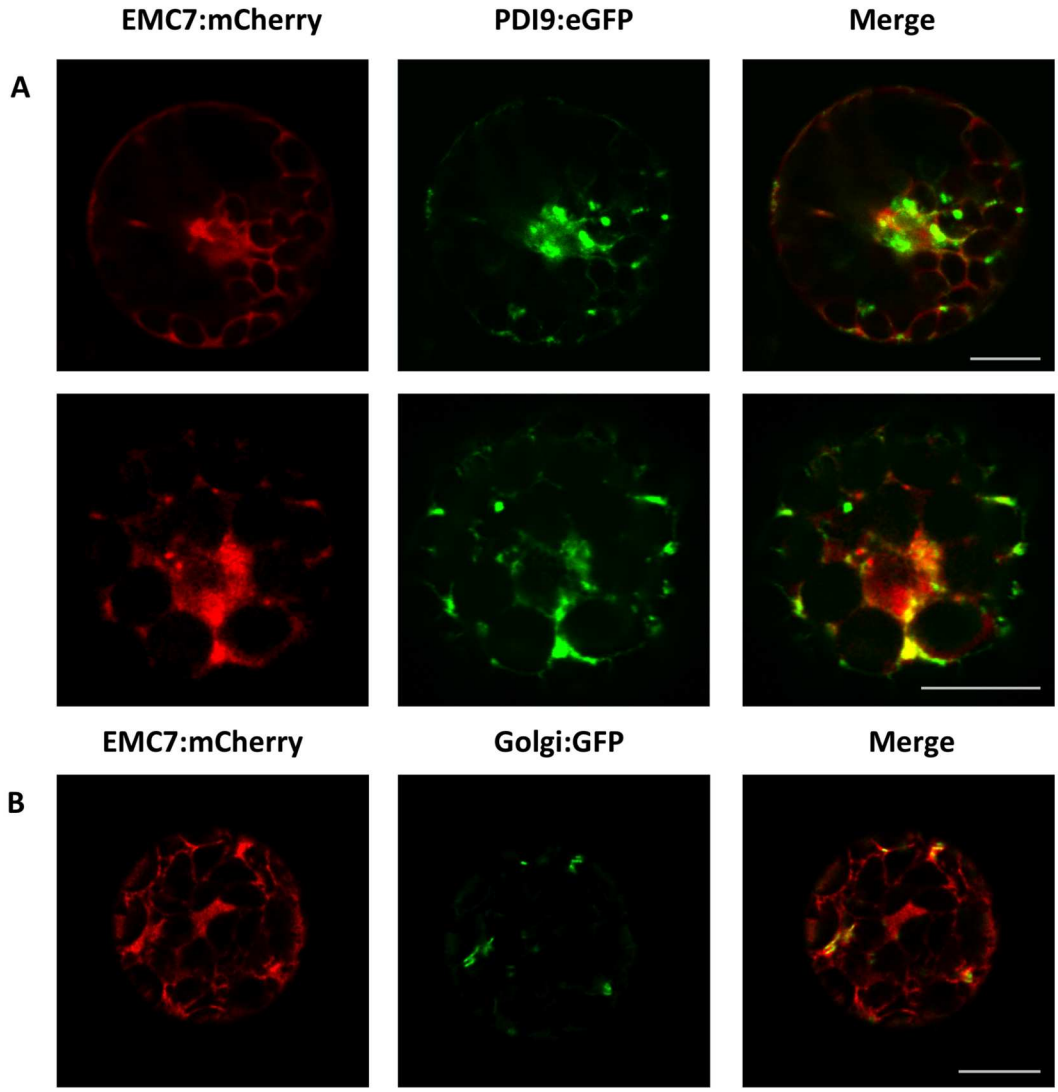

FIGURE 10: EMC7:mCherry partially co-localizes with PDI9:eGFP and shows ER/cis-Golgi labeling. A: PDI9:eGFP column is colored green. EMC7:mCherry is colored red. The Merge column shows the merged fluorescence of PDI9 and either EMC7 or the ER marker, where yellow indicates overlapping fluorescence. B: EMC7 and Golgi body co-localization. Scale bar is 10 um.

As expected, PDI9:GFP is located in the ER and often forms punctate structures (Figure 10A) previously determined to be ER-associated protein bodies (Yuen et al 2013). *EMC7* does not appear to co-localize with the PDI9 protein bodies. However, the merged fluorescences of PDI9:GFP and EMC7:mCherry show partial overlap in the ER. Additional experiments confirmed that EMC7 partially localizes in Golgi bodies (Figure 10B).

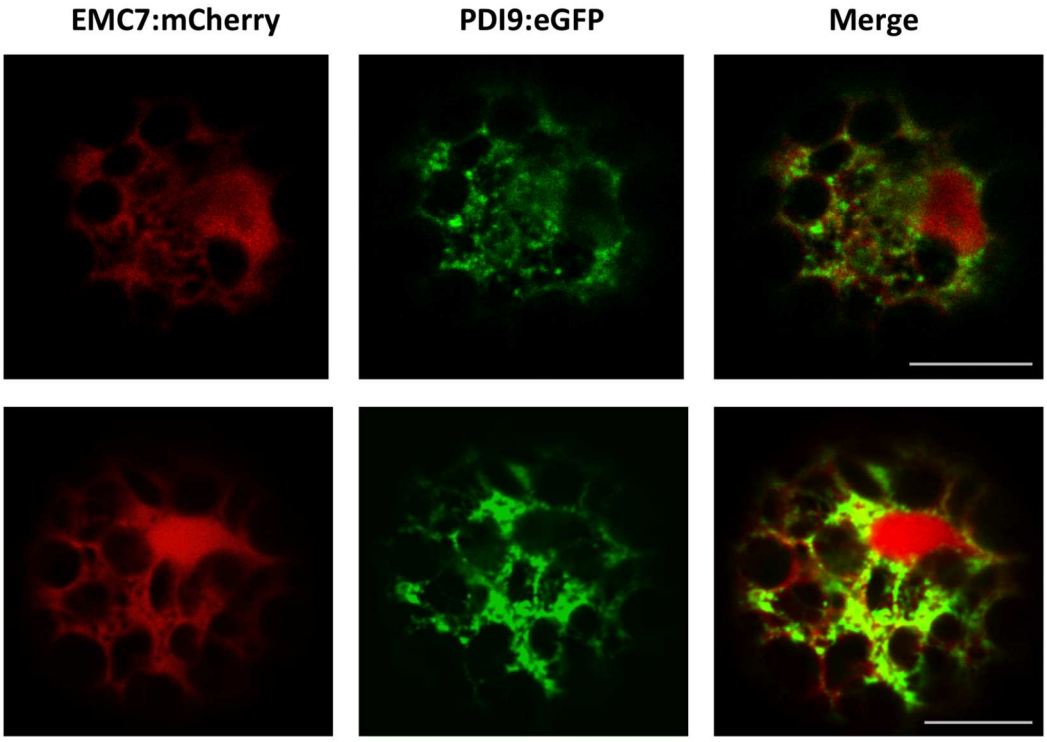

FIGURE 11: EMC7:mCherry localization shows a distinct secondary subcellular location**.** Scale bar is 10 um.

That said, EMC7:mCherry appears to have two subcellular locations. EMC7:mCherry can be seen as both an ER/cis-Golgi protein as well as a cytosolic/nuclear protein as shown in Figure 11. Within the same sample, both expression patterns are present; this has been

demonstrated in two separate experiments. PDI9:eGFP remains similar in both EMC7:mCherry expression types.

LRX8 and PDI9 co-localization

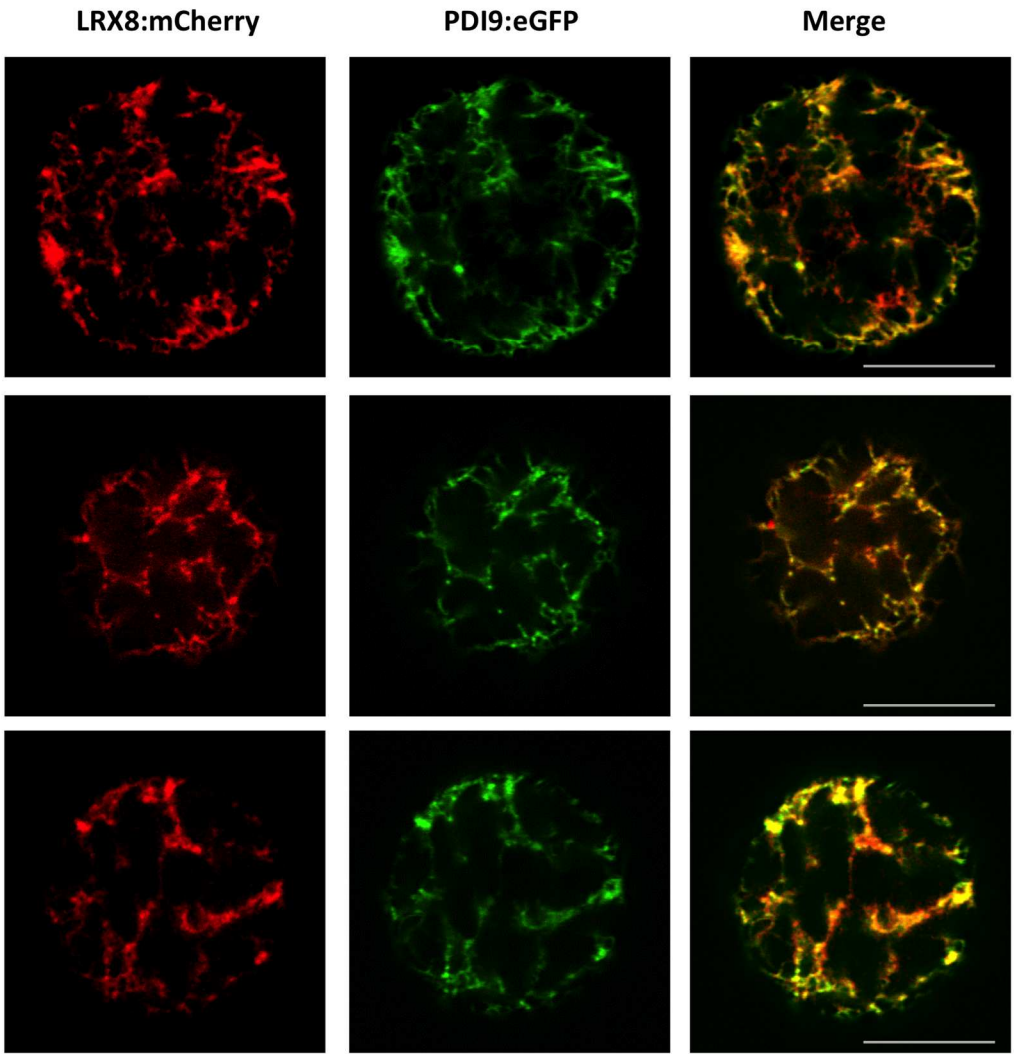

FIGURE 12: LRX8 and PDI9 co-localization in transfected protoplasts. LRX8 is fused to mCherry (red). PDI9 is fused to eGFP (green). Overlap of fluorescence is yellow. Scale bar is 10 um.

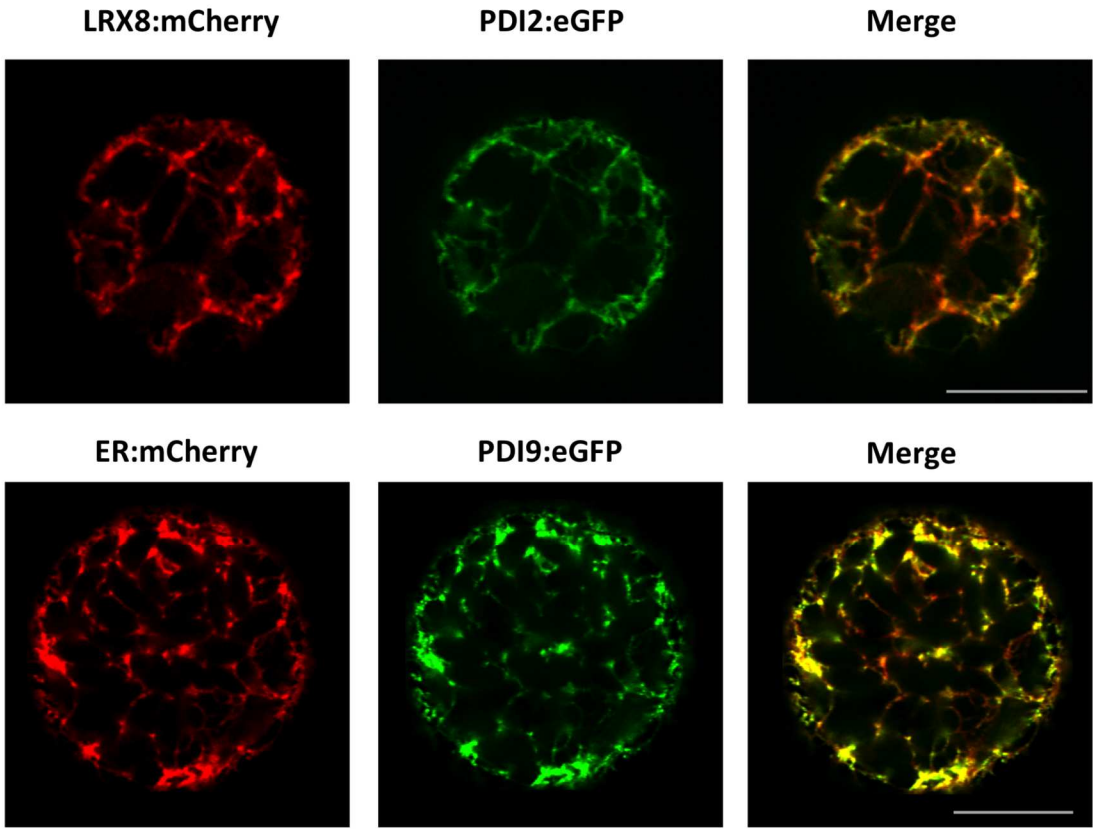

FIGURE 13: LRX8 co-localizes with PDI2, an ER-resident protein. LRX8 and the ER marker are fused to mCherry and colored red. PDI2 and PDI9 are fused to eGFP and colored green. Overlap of fluorescence is false colored yellow. Scale bar is 10 um.

LRX8 strongly co-localizes with PDI9 in the ER. Unlike EMC7, LRX8 usually overlaps where PDI9 punctate are present. As further evidence of LRX8 localizing to the ER, protoplasts were transfected with LRX8:mCherry and PDI2:eGFP. PDI2 is a canonical protein disulfide isomerase- a-b-b'-a' with a KDEL ER retention signal.

Discussion

PDI9 and LRX8 co-localize within the ER in transfected protoplasts. Although LRX8 is a cell wall protein, its signal peptide directs it through the secretory pathway. PDI2 was used as secondary confirmation that LRX8 passes through the ER. Indeed, LRX8 almost fully overlaps with PDI9. However, LRX8 has a small number of punctate that are not co-localized with PDI9 or PDI2. These punctate could be LRX8 entering Golgi bodies on its way to the plasma membrane. LRX8's final subcellular location is anchored to the cell wall. Since protoplast transfection requires the digestion of the cell wall for foreign plasmid DNA to enter the cell, it is not possible to view cell wall proteins in their native location in protoplasts. To visualize the expression of LRX8 in cell walls, a stable transformant would be necessary.

That EMC7:mCherry shows two mutually exclusive expression patterns is puzzling. The EMC7:mCherry fusion used in this experiment is the full coding sequence, including the transmembrane domain. The ER/cis-Golgi labeling is expected based its sequence, as well as the location of mammalian EMC. The cytosolic/nuclear labeling shown in Figure 11 is not representative of a transmembrane or a secretory protein.

One possibility is that the EMC7:mCherry fusion has a cryptic splice site that results in an artifactual truncated transcript lacking the sequence necessary for authentic localization. In other words, the transcript does not have the signal peptide or transmembrane domain to direct EMC7:mCherry to the true location of EMC7. Another possibility is that EMC7:mCherry is being translated in full but is cleaved for reasons unknown. Further research into *EMC7* should include experiments to elucidate its subcellular location. The co-localization data shown here has mCherry fused to the C-terminus of EMC7. To rule out the possibility of post-translational

cleavage of mCherry from EMC7, mCherry could be fused to the N-terminus of EMC7. If the expression pattern is ER/cis-Golgi only and never cytosolic/nuclear, that would suggest that EMC7 truly localizes to the ER. Future experiments could also include Western blotting of isolated microsomes using mCherry antiserum or a generated EMC7 antiserum, to confirm the presence of EMC7 in the ER.

CHAPTER IV: CHARACTERIZATION AND EXPRESSION ANALYSIS OF UPR GENES IN A *PDI9-PDI10* MUTANT

Introduction

As described in Chapter I, the unfolded protein response attempts to alleviate ER stress, primarily through the up-regulation of chaperones and foldases. *PDI9* and *PDI10* are part of the UPR, yet their influence on other members of the UPR is unknown. Mutant analysis provides experimental evidence for the function of specific plant genes. Transgenic plants are invaluable tools for studying single gene effects in plants. In this thesis, both knockout and overexpressor plants are used. Knockout (KO) is defined as the disruption of a gene such that it creates an incomplete mRNA and therefore improper protein product. Overexpression mutants utilize the use of an ectopic constitutive promoter, e.g. the cauliflower mosaic virus (CaMV) promoter 35S described in Chapter III, to create an abundance of mRNA for a target gene. Knockout plants allow biologists to study how cells function in the absence of a certain protein, whereas overexpression demonstrates the effect of an excess amount of a target gene. Prior to this thesis, knockouts of *pdi9-1*, *pdi10-1* and double knockout *pdi9-pdi10* were created. Additionally, a *PDI9* overexpressor (*PDI9* OE) was created by transforming WT plants with 35S:PDI9 plasmid.

Here, I use knockout plants to understand the effect of the knocked-out genes on ER stress. First, *PDI9* and *PDI10* mutants are characterized at DNA, RNA, and protein levels. Second, wild-type and *pdi9-pdi10* KO seedlings are subjected to chemically-induced ER stress and their expression of UPR genes compared. I hypothesize that *pdi9-pdi10* knockout have an elevated UPR under induced stress conditions.

Methods

Authenticating previously created PDI9 and PDI10 mutants

To verify each mutant is homozygous for its intended mutation, PCR, reverse transcription PCR (RT-PCR), and western blotting of *PDI9* were compared to Col-0 wild-type (WT). DNA and RNA were isolated from 7-day-old seedlings using Nucleospin Plant II and RNA Plant, respectively, from Machery Nagel. Protein was isolated from whole 7-day-old seedlings as described (Martínez-García et al. 1999). Ten seedlings each were ground in a 1.5 mL microcentrifuge tube with 100 uL Buffer E (125 mM Tris-HCL pH 8.8, 1% SDS, 10% glycerol, 50 mM NaS_2O_5). After homogenizing tissue, samples were centrifuged (10 minutes at 18,000 g) and the supernatant was saved. Samples were diluted with 1/10 volume Buffer Z (125 mM Tris-HCl pH 6.8, 12% SDS, 10% glycerol, 22% BME, 0.001% bromophenol blue) for analysis via SDS-PAGE.

The schematic diagram in Figure 14 shows the expected T-DNA insertions the single *PDI9* and *PDI10* mutants. The *pdi9-1* mutant is WiscDsLox445A08. Its T-DNA insertion is in the fifth intron at nucleotide position 1736 of 3319 The *pdi9-2* mutant is GK-637C09. Its T-DNA insertion is in the ninth exon at nucleotide position 2778 of 2219. The *pdi10-1* mutant is SALK_206219C. The T-DNA insertion is within the first exon at nucleotide position 121 of 2,574. Two *pdi9-pdi10* double knockouts, named 27A and 60A, were created by crossing *pdi9-1* and *pdi10-1* prior to this thesis. The double knockout used all other experiments in this thesis is 27A.

PCR reactions from genomic DNA were as follows: 7 uL ddH_2O, 1 uL 10 mM forward primer, 1 uL 10 mM reverse primer, 1 uL genomic DNA (about 20 ng DNA), 10 uL 2X Bio-X-

ACT Short Mix (Bioline Cat #: BIO-25026). PCR conditions were as follows: 98ºC 2 minutes; 98ºC 15 seconds, 60ºC 30 seconds, 72ºC 1 minute for 30 cycles; 72ºC 10 minutes.

To test for the presence of *PDI9* and *PDI10* transcripts, first strand cDNA was synthesized from RNA as described (Krug and Berger 1987). 2 ug RNA were incubated with 0.5 ug oligo dT in RNase-free ddH_2O at 70ºC for 5 minutes. Samples were briefly incubated on ice while first strand cDNA mix was added: 5 uL 5X MMLV buffer, 1.25 uL 10 mM dNTP, 0.63 uL 40 units/uL RNason Plus, 1 uL 200 units/uL MMLV reverse transcriptase, 2.12 uL RNase-free ddH_2O. First strand cDNA reaction was at 42ºC for one hour. RT-PCR reactions were as follows: 7 uL ddH_2O, 1 uL 10 mM forward primer, 1 uL 10 mM reverse primer, 1 uL cDNA, 10 uL 2X Bio-X-ACT Short Mix.RT-PCR conditions were as follows: 98ºC 2 minutes; 98ºC 15 seconds, 60ºC 30 seconds, 72ºC 1 minute for 30 cycles; 72ºC 10 minutes.

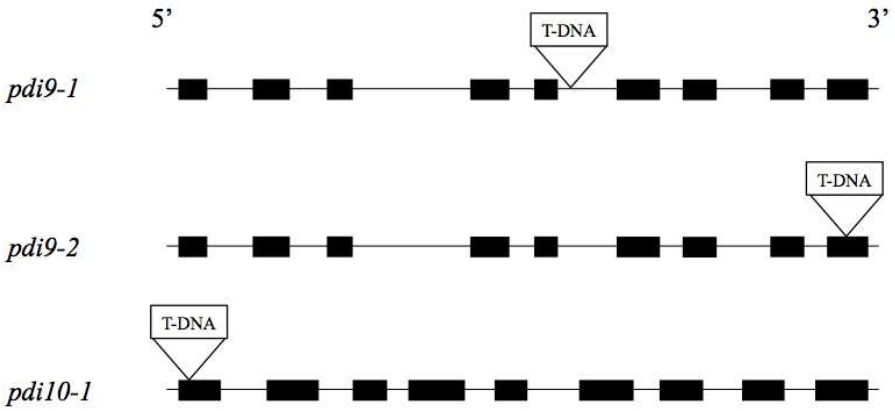

FIGURE 14: T-DNA insertions for *pdi9-1, pdi9-2*, and *pdi10-1* mutants. Rectangles indicate an exon. The *pdi9-1* mutant is WiscDsLox445A08 and its T-DNA insertion is 1,608 nucleotides after the start codon. The *pdi9-2* mutant is GK-637C09 and its insertion is 2,653 nucleotides after

the start codon. The *pdi10-1* mutant is SALK_206219C and its insertion is 20 nucleotides after the start codon.

TABLE 3: Primer sequences for genotyping and RT-PCR

Primer	**Sequence**
WiscDsLoxP745	AACGTCCGCAATGTGTTATTAAGTTGTC
Lba1	TGGTTCACGTAGTGGGCCATCG
GK-8474	ATAATAACGCTGCGGACATCTACATTTT
PDI9g_F	ATGTATAAATCACCATTAACGTTGC
PDI9g_R	TCACAACTCATCCTTAGAACCAAC
PDI10g_F	GCTTTGAAGGCACCAGAATGTGG
PDI10g_R	TATGGACAAACCTGCTTGATAGC
PDI9rt_F	ATGTATAAATCACCATTAACGTTGC
PDI9rt_R	TCACAACTCATCCTTAGAACCAAC

Primers are shown in Table 3. WisDsLoxP745 is the left border primer for the *pdi9-1* T-DNA insertion; Lba1 is for *pdi10-1* and *GK-8474* is for *pdi9-2*. The PDI9g_F and R were used to amplify *PDI9* from genomic DNA and PDI9rt_F and R used for RT-PCR. PDI10g_F and R were used for both genomic DNA and cDNA for *PDI10.*

Quantitative PCR (qPCR) of UPR genes in chemically-stressed seedlings

The effect of chemically-induced ER stress on WT and *pdi9-pdi10* knockout seedlings was done as described (Lu and Christopher 2008). 25 seeds of each type were grown in 50 mL of 1X liquid LS media after stratification for 24 h. Flasks were shaken at 50 rpm at 22 C, with 16 h/8 h light/dark. After 7 days, stressed samples were exposed to 10 mM DTT for 5 h. After treatment, RNA was isolated from all samples using the RNA Plant kit from Machery Nagel.

Prior to qPCR, semi-quantitative reverse-transcription PCR (RT-PCR) was done for all samples and genes. First strand cDNA was synthesized from RNA as described earlier. bZIP60 primers are described by Nagashima et al (2011) and shown in Figure 15. qPCR primers were designed using Primer3 (v. 0.4.0) to identify amplicons around 200 bp with a melting point around 63 C. An alternative bZIP60s forward primer was used, "q-bZIP60sF" instead of the previously reported forward primer, to make each qPCR amplicon equal in size and melting point.

TABLE 4: Primers for qPCR

Primer	**Sequence**
BiP2_F	CCAAGACCAGCAGACCACCG
BiP2_R	CCACTCGCCTTGTCCTCTGC
PDI6_F	GGTCAGCGAGCGGAAATGTTG
PDI6_R	TACAGCTCGTCCTTTGCGGC
PDI11_F	CGTTACTCGCGTTGCTTCTGG
PDI11_R	TGACCACACCAGGGAGCGTA
Actin2_F	TCCTTGTACGCCAGTGGTCG
Actin2_R	CCGCTCTGCTGTTGTGGTGA
bZIP60iF	CCAGTCTCTACGTTACTGTTTGCAAAAGGGTAATGGC
bZIP60iR	GCAAATGAAGTTTACTCCCAGAAGCCAAAGCAGG
bZIP60sF	TGATGATGACGAAGAAGGAGACGATGATG
q-bZIP60sF	TCGTTGAGTGCTTCGTTGCTG
bZIP60sR	AGGGAACCCAACAGCAGACTCC

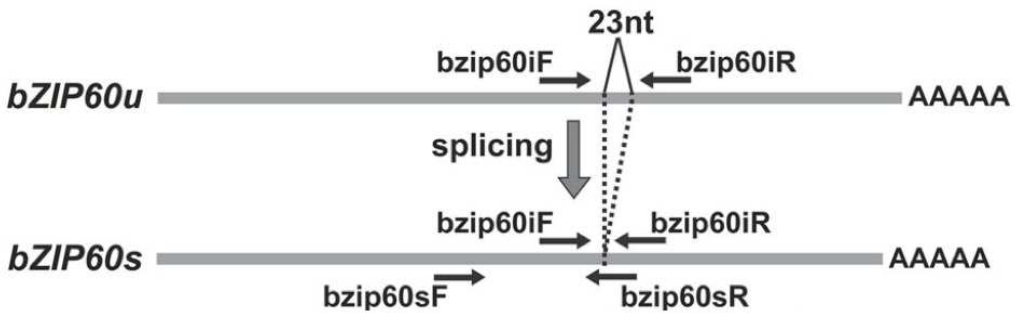

FIGURE 15: Primer locations for bZIP60 unspliced (bZIP60u) and spliced (bZIP60s). bZIP60iF and iR amplify both spliced and unspliced bZIP60 transcripts. bZIP60sR is and bZIP60sF2 are designed through the spliced region such that only spliced bZIP60 can be amplified when using those primers. Figure from Nagashima et al. (2011).

qPCR was done by Dr. Tiirikainen's lab at the University of Hawai'i Cancer Center. Data analysis was done using the $2(-\Delta\Delta CT)$ method as described, using Actin2 as the housekeeping gene for normalized expression (Livak and Schmittgen 2001). One-way ANOVA was used for statistical analysis.

Results

Genotyping and RT-PCR of PDI9 and PDI10 mutants

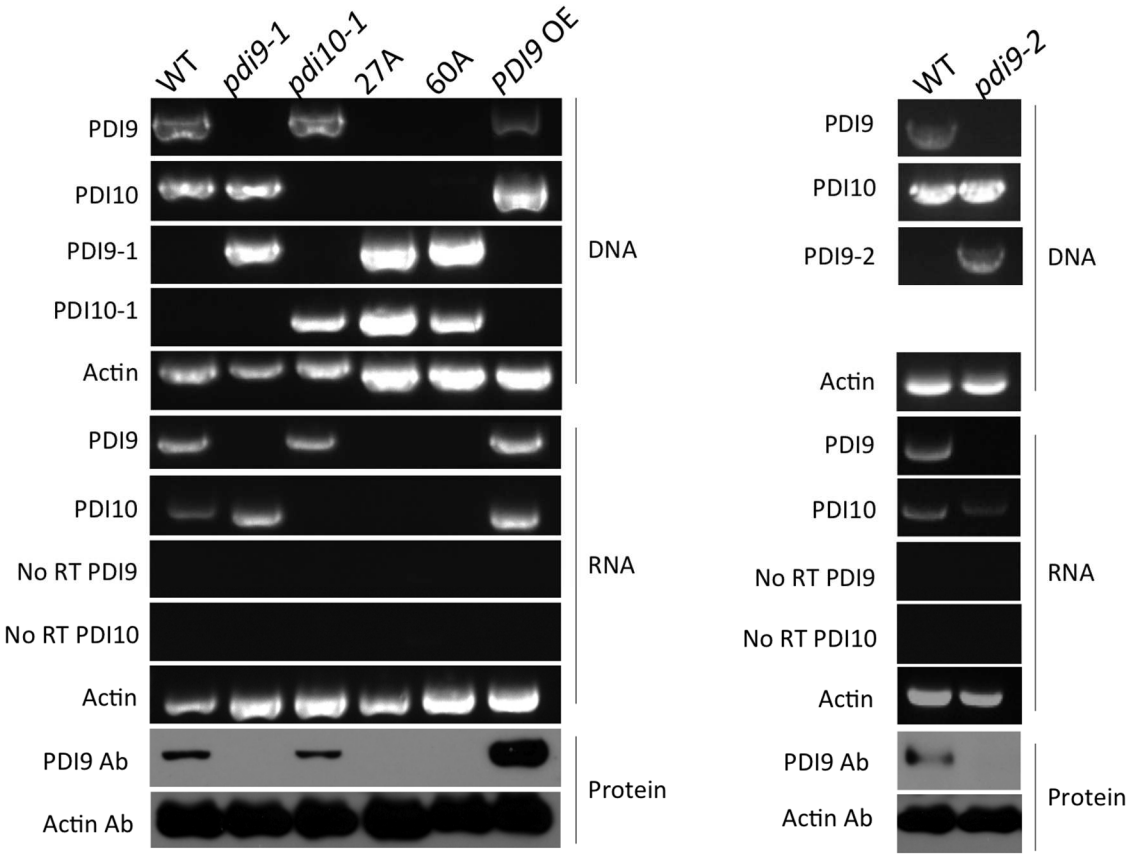

FIGURE 16: Characterization of *PDI9* and *PDI10* genotypes. PDI9-1 is the T-DNA insert for *pdi9-1,* PDI10-1 is the T-DNA insert for *pdi10-1,* and PDI9-2 is the T-DNA insert for *pdi9-2*.

Figure 16 demonstrates that the *PDI9* and *PDI10* mutants are authentic. The *pdi9* and *pdi10* single knockouts lack the *PDI9* and *PDI10* gene, respectively, and have the appropriate T-DNA insertion in genomic DNA. The *pdi9-pdi10* double knockouts 27A and 60A have neither the *PDI9* or *PDI10* genes and have both T-DNA inserts. The 35S:PDI9 overexpressor OE has

both *PDI9* and *PDI10* genes. Western blotting with anti-*PDI9* shows the expected presence and absence of PDI9 in each of the mutants: WT and pdi10 have approximately equal amounts of PDI9 protein, whereas OE shows a relative abundance of PDI9. The *PDI9* and *PDI10* mutants are thereby genuine and appropriate for use in experiments.

qPCR of UPR transcripts in ER-stressed seedling

TABLE 5: The normalized expression (%) of given UPR transcripts relative to housekeeping gene (HKG) Actin2 for given genotype-treatment. *bZIP60i* includes both spliced and unspliced *bZIP60*. *: $p < 0.01$ for n=3. +: *bZIP60u* is a calculation of unspliced bZIP60, i.e. *bZIP60i* minus *bZIP60s*, and is not a directly measured transcript.

	Untreated		**Treated**	
	WT	**KO**	**WT**	**KO**
BiP2	160 ± 33.5	446 ± 35.3*	2077 ± 143.5	2635 ± 78.0
PDI11	75 ± 13.7	177 ± 24.2*	401 ± 29.4	359 ± 127.4
PDI6	8 ± 1.4	20 ± 2.5*	119 ± 26.6	103 ± 23.3
bZIP60i	56 ± 6.0	98 ± 33.8	395 ± 94.1	442 ± 72.0
bZIP60s	3 ± 0.2	5 ± 0.7	39 ± 8.3	50 ± 20.4
bZIP60u^{+}	53	356	93	392

As expected, the UPR was induced in both WT and the DKO upon treatment with DTT as evident by the large increase in expression of *BiP2, PDI6, PDI11*, and *bZIP60s* (Table 5).

Surprisingly, the expression of three UPR genes- *BiP2, PDI6*, and *PDI11*- was significantly increased in the KO untreated relative to WT untreated. *BiP2* expression increased 270% in the DKO untreated relative to WT untreated. *PDI6* and *PDI11* increased 250% and 235% in the DKO untreated relative to WT untreated, respectively. There is no significant difference, however, between the two genotypes when treated with DTT. Additionally, *bZIP60u* and *bZIP60s* was not significantly different between WT and the DKO in either untreated or treated conditions.

Discussion

In the *pdi9-pdi10* double knockout, non-stressed plants have increased expression of UPR genes relative to wild-type. Lu and Christopher (2008) thoroughly characterized the role of the PDI family during ER stress: *PDI6* and *PDI11* were known to be up-regulated alongside *PDI9* and *PDI10. BiP2* and *bZIP60* were significantly up-regulated as well. In this experiment, some, but not all, of the UPR genes were induced in the *pdi9-pdi10* double knockout. *PDI6, PDI11*, and *BiP2* were significantly more expressed in non-stressed plants than wild-type, but *bZIP60* was not.

That bZIP60, spliced or unspliced, is not significantly different in unstressed conditions while other UPR genes are suggests a handful of hypotheses. First, *PDI6* and *PDI11* are compensating for the role of *PDI9* and *PDI10* during normal cellular processes. *PDI6* is homologous to PDI5 in Arabidopsis and canonical PDI in yeast and mammals, making it a well-established chaperone and protein foldase in the ER. PDI11 does not have a true ER retention signal, yet it does have two active "CGHC" sites with two "a" domains in proximity (without a

"b" domain or two in between) as do *PDI9* and *PDI10*. This may explain why these select PDIs are up-regulated in unstressed *pdi9-pdi10* DKO plants.

Future experiments may look at the expression of other PDI family members to further test this hypothesis. The increase in BiP2 in the double KO may reflect an increased need for binding unfolded proteins in the ER. The proteostatic imbalance due to reduced disulfide isomerization at least partially explains the induction of other *PDI*s and *BiP2*. This experiment demonstrates a novel compensation of protein folding activity by non-homologous *PDI*s in *Arabidopsis* and the need to upregulate other chaperones.

Second, if PDI9 binds IRE1 to attenuate the UPR as its homolog does in mammals, the absence of PDI9 leads to misregulation of the UPR in even non-stressed conditions. Eletto et al (2014) demonstrates the PDIA6 is responsible for "turning off" the UPR when ER stress is relieved and that *pdia6* KOs have constitutively expressed UPR. I originally hypothesized that *pdi9-pdi10* double KO plants would have increased expression *bZIP60s* due to an inability to turn off IRE1's signaling of ER stress. However, it seems likely that *PDI6* and *PDI11* are at least partially induced by a separate UPR transcription factor to mitigate the absence of *PDI9* and *PDI10*. Nevertheless, these findings are consistent with Eletto et al. (2014) in that the *pdi9-pdi10* double knockout shows elevated UPR transcripts in non-stressed conditions. PDI9 may bind IRE1 to regulate the UPR in ways not wholly accounted for in this experiment. Co-immunoprecipitation of IRE1 and PDI9 is necessary to confirm the binding activity and function in plants.

Male reproductive tissues, particularly the tapetum, must maintain a high throughput of secretory proteins for pollen development. Members of the ER stress response are precisely

regulated as pollen matures. Since *pdi9-pdi10* KO seedlings are presumably facing ER stress in non-stressed conditions, it follows that male reproduction would be especially sensitive. This experiment suggests that double KO pollen will have an induced UPR exceeding wild-type in non-stressed conditions. Furthermore, heat-stressed double KO pollen is expected to be less capable of meeting protein-folding demands to the point that it disrupts normal pollen development. Future work should include quantitative real-time PCR of UPR transcripts in *pdi9* mutant pollen grains in non-stressed and heat-stressed conditions to uncover transcriptome changes.

CHAPTER V: HEAT STRESS PHENOTYPING OF REPRODUCTIVE TISSUES OF *PDI9* AND *PDI10* MUTANTS

Introduction

Chapter I discussed the importance of proteostasis for proper reproductive development, in particular the role of the UPR for the development of pollen under heat stress. Identifying and measuring phenotypes of male gametophytes is complicated by logistic and genetic challenges. First, harvesting sufficient *Arabidopsis* pollen for phenotyping is not a small task. The former McCormick lab established guidelines for robust statistical analysis of Arabidopsis pollen. A "rapid" evaluation of 1000 plants, minimum two flowers of the same developmental stage from each plant, should be scored individually on slides by manually splaying flowers to release pollen (Johnson-Brousseau and McCormick 2004). This is by no definition a rapid evaluation and requires a significant investment of time on a microscope. The paper also provides methods for large-scale isolation using a homemade three-filter vacuum system that can isolate dehisced pollen from large flats of plants. This pellet of pollen is useful for DNA, RNA or protein isolation, but is less amenable to physical phenotyping.

Mutations to pollen affect the haploid life cycle, which results in segregation distortion. As such, it can be difficult to isolate a genuine homozygous mutant, despite the fact that pollen phenotypes can occur in heterozygous mutants. This is further complicated by separate female gametophytic mutations or downstream sporophytic mutations originating with a haploid abnormality. More recent work has demonstrated epigenetic cross-talk between gametophytic and sporophytic tissues that leads to complex mutations manifesting in a later alternating

generation (Carter et al. 2016). In other words, pinpointing the genetic origin of a phenotype present in pollen requires analysis of several tissues and mutants.

Traditional Alexander viability staining requires chloral hydrate and phenol, both of which are harmful to human health. Though useful, the original Alexander staining protocol was a tedious process that took over 24 h (Alexander 1969). Peterson et al. (2010) described an improved fixing and staining protocol that avoids the use of those two chemicals. However, their protocol still requires fixation with Carnoy's fixative (6 alcohol:3 chloroform:1 acetic acid) prior to staining. This step adds minimum two hours to the process and requires careful removal of the fixative before staining. Finally, the sample is imaged in undiluted stain solution, which risks over-staining the sample and obscuring the difference between aborted and non-aborted pollen.

In this chapter, I detail an improved and high-throughput method to quantify pollen viability and pollen counts in order to characterize *PDI9* and *PDI10* mutants and observe for a phenotype. Time from pollen harvest to microscope can be done in as little as half an hour with this high-throughput method. I also demonstrate that fixation is not required for differentiation of aborted and non-aborted *Arabidopsis thaliana* pollen grains. Finally, I created a simple ImageJ macro that allows rapid counting of total pollen grains from photographs that reduces analysis time.

Using a combination of light and scanning electron microscopy, pollen can be precisely and efficiently phenotyped. Furthermore, I explore the downstream developmental impacts and structural features of reduced pollen viability and dehiscence under heat stress. Finally, I propose a role for *PDI9* and *PDI10* during heat-stressed pollen development.

Methods

Characterizing PDI9 *expression in floral tissues*

Isolating proteins from floral tissues was done by adapting several protocols (Chang and Huang 2017; Johnson-Brousseau and McCormick 2004; Martínez García et al. 1999). Pollen was most efficiently harvested by vortexing whole flowers in buffer in a 50 mL conical tube, then filtering excess plant material with MiraCloth (EMD Millipore Cat #: 475855-1R). Pollen was centrifuged, pelleted, and ground in K-HEPES buffer (20 mM HEPES pH 7, 10 mM K-acetate, 2 mM MgCl2, 0.1% Tween 20, 0.2% Triton X-100, 1 mM PMSF). Anthers were removed from harvested flowers using fine-tipped forceps (Rubis Cat #: DV-30) dipped in liquid nitrogen, then ground in Buffer E (as described in Chapter IV). Five whole flowers were ground in a 1.5 mL microcentrifuge tube in 100 uL Buffer E. Buffer Z with B-ME was added to samples prior to SDS-PAGE.

Heat stress treatment

Seedlings were grown on 0.5X LS with 3% sucrose media (Phyto Technolgy Laboratories Cat #: L473) for 7 days and transplanted to individual pots that had a randomized location within a flat. All plants were grown at 22ºC on a 16/8 h of light/dark cycle ((approximately 75 μmol photons m^{-2} s^{-1})for two weeks. 2.5 weeks after transplanting, approximately half of the plants were moved to a growth chamber for heat stress, while the other half remained in normal growth conditions. Heat-stressed plants were exposed to 35/27 ºC 16/8 h while the control plants remained at 22 ºC. Pollen harvest took place after 2 weeks of heat stress.

It should be noted that less severe prolonged heat stress regimes were tested and yielded positive data but will be excluded due to redundancy.

High-throughput pollen viability assay using a modified Alexander stain

TABLE 6: Comparison of pollen viability staining methods

	Alexander (1969)	**Peterson et al. (2010)**	**High-throughput method**
Use of highly toxic chemicals	Yes	No	No
Harvest	Individual anthers mounted on slides	Individual anthers mounted on slides	Pollen isolated from whole flowers directly in staining solution
Fixation prior to staining	No	Yes, minimum two hours	No
Staining	Up to 48 hours at 50^{o}C	30 seconds over alcohol burner	1 minute while vortexing, no heat required
Total time per sample	24-48 hours	About 2 hours	About 30 minutes
Pollen quantitation	Manual	Manual	Semi-automated using ImageJ

Table 6 highlights the differences between the original Alexander staining protocol, improvements made by Peterson et al. (2010), and the high-throughput method described in this thesis. Harvesting pollen directly into staining solution and avoiding the fixation step saves nearly two hours per sample. I confirmed that fixation was not required for *Arabidopsis thaliana* pollen by comparing the differential staining of fixed and unfixed pollen and found no change in the ability to distinguish aborted and non-aborted pollen.

Modified staining solution:

The modified Alexander stain is described (Peterson et al. 2010). The following stock solutions were stored in the dark: 1% (w/v) malachite green in 95% ethanol, 1% (w/v) acid fuchsin in ddH_2O, and 1% orange g (w/v) in ddH_2O. Staining solution was prepared from the aforementioned stock solutions in the order given below:

Stain solution (50 mL):
1. 5 mL 95% ethanol
2. 500 uL malachite green solution
3. 25 mL ddH_2O
4. 12.5 mL glycerol
5. 2.5 mL acid fuchsin solution
6. 250 uL orange g solution
7. 2 mL glacial acetic acid
8. 2.25 mL dI water

Harvest and staining:

Individual *Arabidopsis* stage 13 flowers (as defined Smyth et al. 1990) were harvested and placed in 1.5 mL microcentrifuge tubes. 150 uL of Alexander staining solution was added immediately before vortexing. Each tube was vortexed on high for one minute to release the pollen from anthers before centrifugation for 2 minutes at 18,000 x g. Flowers were carefully removed with a fresh pipette tip 200 uL to avoid disturbing the pollen pellet. 100 uL of solution was removed, leaving 50 uL of the original stain. 750 uL of ddH_20 was added and each sample briefly vortexed to wash pollen. Samples were centrifuged and washed twice with 750 uL ddH_20. After the last wash, all but 25 uL of solution was removed. Pollen was resuspended in the 25 uL and the total volume was used for imaging.

Imaging and analysis:

Glass slides (Electron Microscopy Sciences Cat #: 71878-01) with 1.6 mm depth wells were used to image pollen. Slides were loaded onto an Olympus BHB light microscope and photographed using an AmScope WF200 camera. Pollen was counted from photographs at 4X or 10X with a custom Javascript utilizing built-in macros (example given below). Each image was converted to a 16-bit image using default thresholds and pollen grains were identified from a defined minimum pixel size. Each pollen count was overlaid on the original RGB image. Aborted and clustered pollen grains were manually counted from the processed image. Each pollen grain is classified as non-aborted (viable), aborted (non-viable), or ambiguous. One-way ANOVA was chosen for statistical analysis and calculated using Microsoft Excel.

ImageJ macro (in Javascript) for counting pollen at 4X magnification:

```
roiManager("reset");
close("*");
dir = getDirectory("Please choose a directory:");
list = getFileList(dir);

for (i = 0; i < list.length; i++)
{
        open(list[i]);
        run("Duplicate...", "title=copy");
        selectWindow(File.getName(list[i]));
        run("16-bit");
        setAutoThreshold("Default no-reset");
        setOption("BlackBackground", false);
        run("Convert to Mask");
        run("Analyze Particles...", "size=125-Infinity show=Overlay display summarize add");
        // Change size to 500 for counting at 10X
        Overlay.copy;
```

```
        selectWindow("copy");
        Overlay.paste;
        run("Flatten");
        selectWindow(File.getName(list[i]));
        close();
        selectWindow("copy");
        close();
        waitForUser("Record aborted and clustered pollen\nClick OK when done");
        roiManager("reset");
        close("*");
}

close("*");
```

Heat-stressed pollen scanning electron microscopy

For qualitative imaging, two to six Stage 13 flowers from each genotype-treatment were harvested. Anthers from harvested flowers were gently dabbed directly onto the mounting medium to release pollen. Pollen grains and anthers were gently secured to the carbon mounting using a handmade tool (eyelash attached to a small dowel rod) under a dissecting microscope. Specimens were mounted with conductive carbon tape (Electron Microscopy Sciences Cat. #: 77827-12) on aluminum stubs (Ted Pella Cat. #: 16111) and sputter coated with gold/palladium (Anatech USA Cat. #: 1002021) in a Hummer 6.2 sputter coater. Specimens were viewed with a Hitachi S-4800 Field Emission Scanning Electron Microscope at an accelerating voltage of 5.0 kV at 4,000 and 11,000 magnifications

Heat-stressed silique phenotyping

After the heat stress described above, heat-stressed plants were moved to the control (22^{o}C) environment with 16/8 h light/dark for one week. Siliques were harvested using Bac-

Molenaar (2015) as a starting point. Ten and twenty siliques from the main stem were harvested from control plants and heat-stressed plants, respectively. Photos of siliques were taken with a ruler in frame for calibration and measurement in ImageJ.

Results

Western blotting of floral proteins from select PDI9 *mutants*

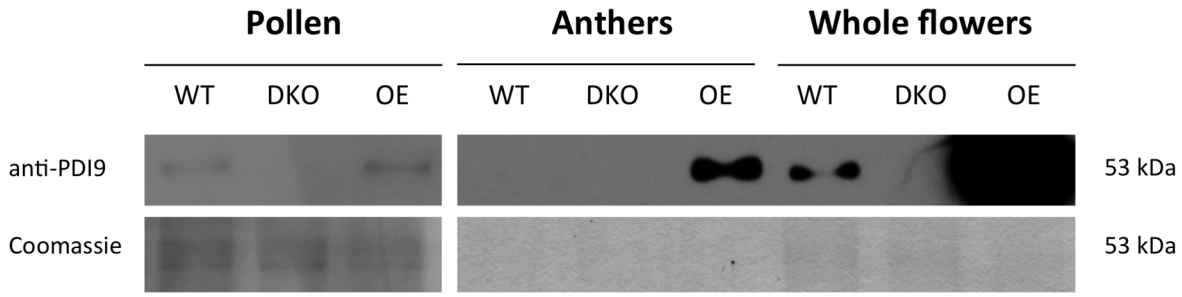

FIGURE 17: Western blotting of floral tissues with PDI9 antiserum. Pollen blotting conditions: 1:100 anti-PDI9, 1:3,000 anti-rabbit secondary, 10 ug per lane, 45 minute exposure. Whole flower and anther blotting conditions: 1:100 anti-PDI9, 1:3,000 anti-rabbit secondary, 2.5 ug per lane (anthers) or 10 ug per lane (whole flowers), 30 minute exposure.

To confirm the abundance of PDI9 protein demonstrated by Pro_{PDI9}:GUS expression, protein was isolated from WT, *pdi9-pdi10* DKO, and *PDI9* OE floral tissues. Figure 17 shows that the *PDI9* OE has a greater amount of PDI9 in whole flowers and anthers relative to WT. PDI9 is not detected in WT anthers but is abundant in *PDI9* OE anthers. Additionally, WT and *PDI9* OE pollen have lower amounts of PDI9 than whole flowers of the same genotype. As expected, the DKO does not have any PDI9 protein in its floral tissues. Based on these data, PDI9 is highly expressed in whole flowers and moderately expressed in pollen.

High-throughput Alexander staining of heat-stressed pollen

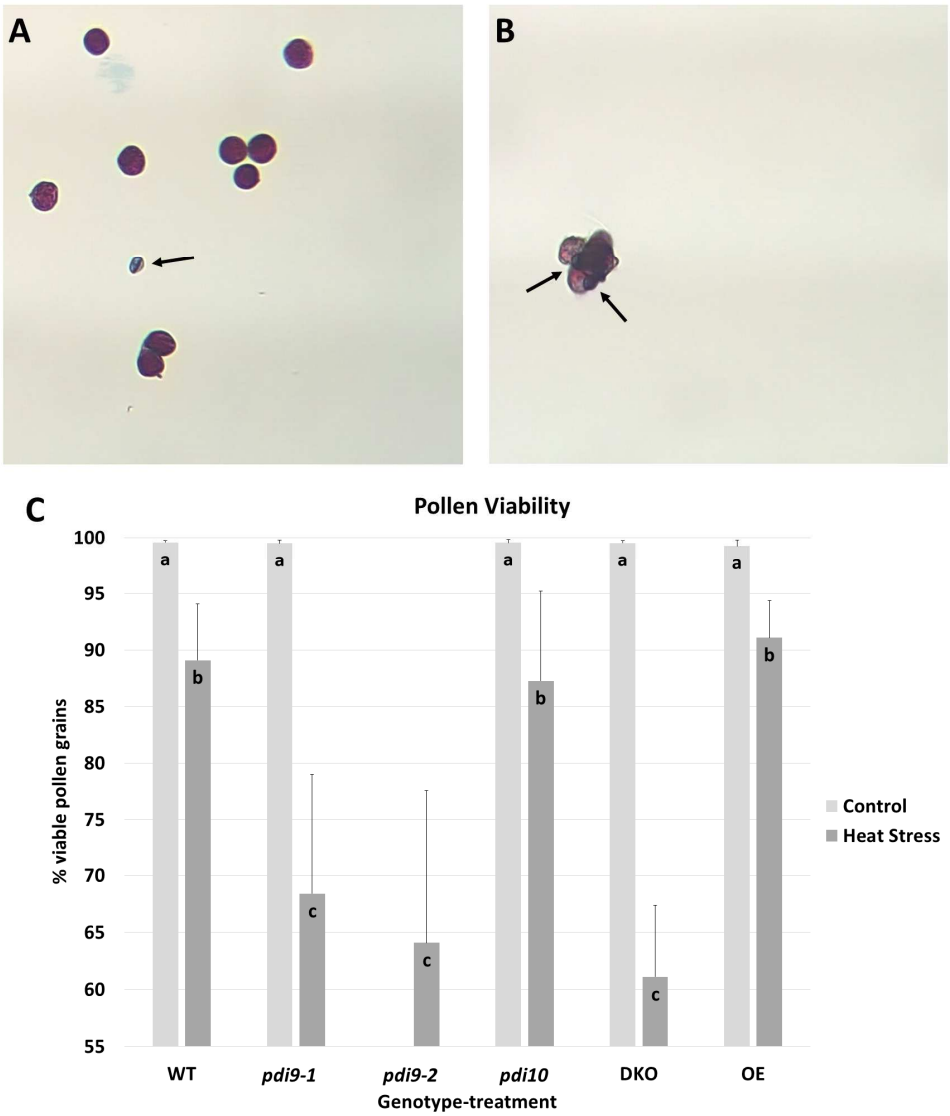

FIGURE 18: *PDI9* is critical for the development of viable pollen under heat stress. (A) wild-type and (B) *pdi9-pdi10* DKO heat-stressed pollen. Arrows point to aborted pollen grains. C: Histogram showing the percent of total pollen grains for a given genotype-treatment that are viable. Letters indicate significance between samples ($p<0.05$ for n=6 each genotype treatment).

Figure 18 shows the pollen viability under non-stressed and heat-stressed conditions. All genotypes share a control percent pollen viability of about 99%. Additionally, the heat stress treatment results in a significant decrease in viable pollen grains across all genotypes. *pdi10* and *PDI9* OE percent pollen viabilities are not significantly different from wild-type. Importantly, *pdi9-pdi10* DKO plants show a significantly lower percentage of viable pollen grains under heat stress relative to WT. The percent of viable pollen grains in WT under heat stress is 87%, whereas the DKO has 62% viable pollen grains under heat stress. Viability in the *pdi9-pdi10* DKO is significantly different that the single *pdi9* KOs under heat stress.

TABLE 7: The number of dehisced pollen grains for each genotype-treatment. Unstressed control (A) and heat-stressed pollen counts (B) are from three stage 13 flowers per sample. Letters indicate significance between samples ($p<0.05$ for n=6 for each genotype-treatment).

	Control	**Heat stress**
WT	1918 ± 692[a]	277 ± 113 [b]
pdi9-1	1534 ± 454 [a]	69 ± 40 [d]
pdi9-2	N/A	69 ± 33 [d]
pdi10-1	1516 ± 450 [a]	167 ± 74 [bc]
DKO	1912 ± 700 [a]	49 ± 21 [d]
PDI9 OE	1694 ± 689 [a]	149 ± 71 [c]

The modified Alexander staining method described in this thesis allows for the quantification of dehiscent pollen grains per flower. Unstressed plants have approximately 1,700 dehiscent pollen grains per sample, or 570 pollen grains per flower. All genotypes show a

significant reduction in the number of dehisced pollen grains under heat stress, as shown Table 7. The *pdi9* and *pdi9-pdi10* knockouts have a significantly lower number of pollen grains than WT under heat stress. WT plants show an 88% reduction in dehiscent pollen when subjected to heat stress. *pdi9-1* single KO and *pdi9-pdi10* double KO plants have a 97% and 98% reduction in dehiscent pollen, respectively. In other words, flowers lacking *PDI9* dehisce just over a dozen pollen grains per flower under heat stress. Surprisingly, the heat-stressed *PDI9* OE has significantly fewer pollen grains than wild-type.

SEM of heat-stressed pollen

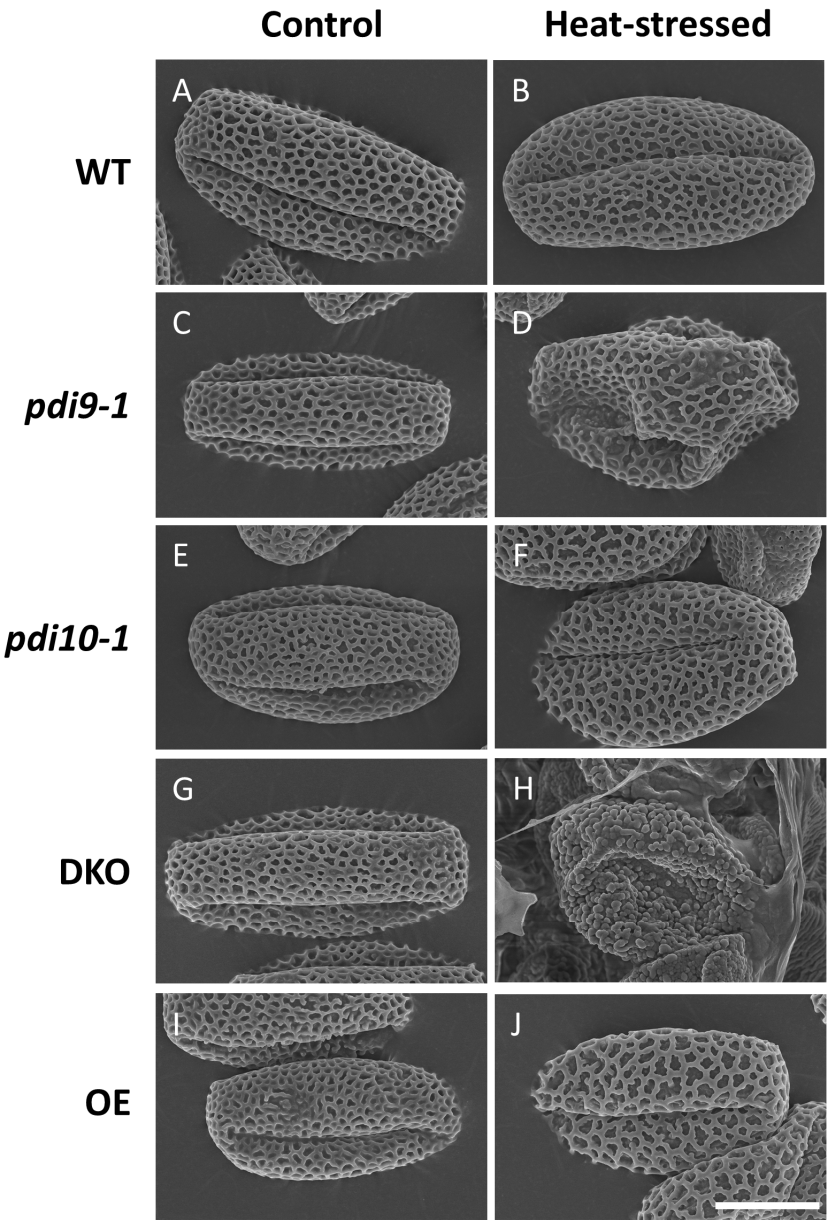

FIGURE 19: Scanning electron micrographs of pollen grains. Each micrograph is a representative pollen grain from control (A,C,E,G,I) and heat-stressed (B,D,F,H,J) plants. Wild-type (A,B), *pdi9-1* (C,D), *pdi10-1* (E,F), DKO (G,H), and OE (I,J) pollen grains were all observed at 4,000X magnification. Scale bar is 10 um.

Scanning electron microscopy reveals that *PDI9* plays a role in exine development. Unstressed pollen grains from each genotype have essentially the same morphology. The majority of heat-stressed wild-type, *pdi10*, and *PDI9* OE pollen grains maintain a normal shape and exine pattern. A small percentage of pollen grains appear smaller and deflated, much like the stained green pollen grain in Figure 8A. *pdi9* pollen grains are more frequently deformed as shown in Figure 19D. Surprisingly, *pdi9-pdi10* pollen grains are almost exclusively deformed under heat stress. The pollen grains shown in Figure 19H and Figure 23A are actually trapped within the anther. The only dehisced pollen was shriveled and stuck together (Figure 23B). The absence of both *PDI9* and *PDI10* dramatically disrupts the development and release of pollen under heat stress.

Furthermore, DKO pollen grains have an unusual exine pattern under heat stress. Figure 20G shows a representative DKO exine pattern in non-stressed conditions. It is substantially the same as wild-type, though the tryphine is nearly level with the exine in small patches. Heat stress drastically disrupts exine pattern under heat stress in the double knockout as demonstrated in Figure 20H. The reticulate pattern found in wild-type pollen is completely absent. Instead, clumps of what are likely sporopollenin form on the exterior of the pollen grain. The *PDI9* OE also has a disrupted exine pattern, but unlike the DKO, the defect is visible in non-stressed as well as stressed pollen grains (Figures 20I, 20J and 21). OE pollen grains have large patches of smooth exine or broken exine reticulua.

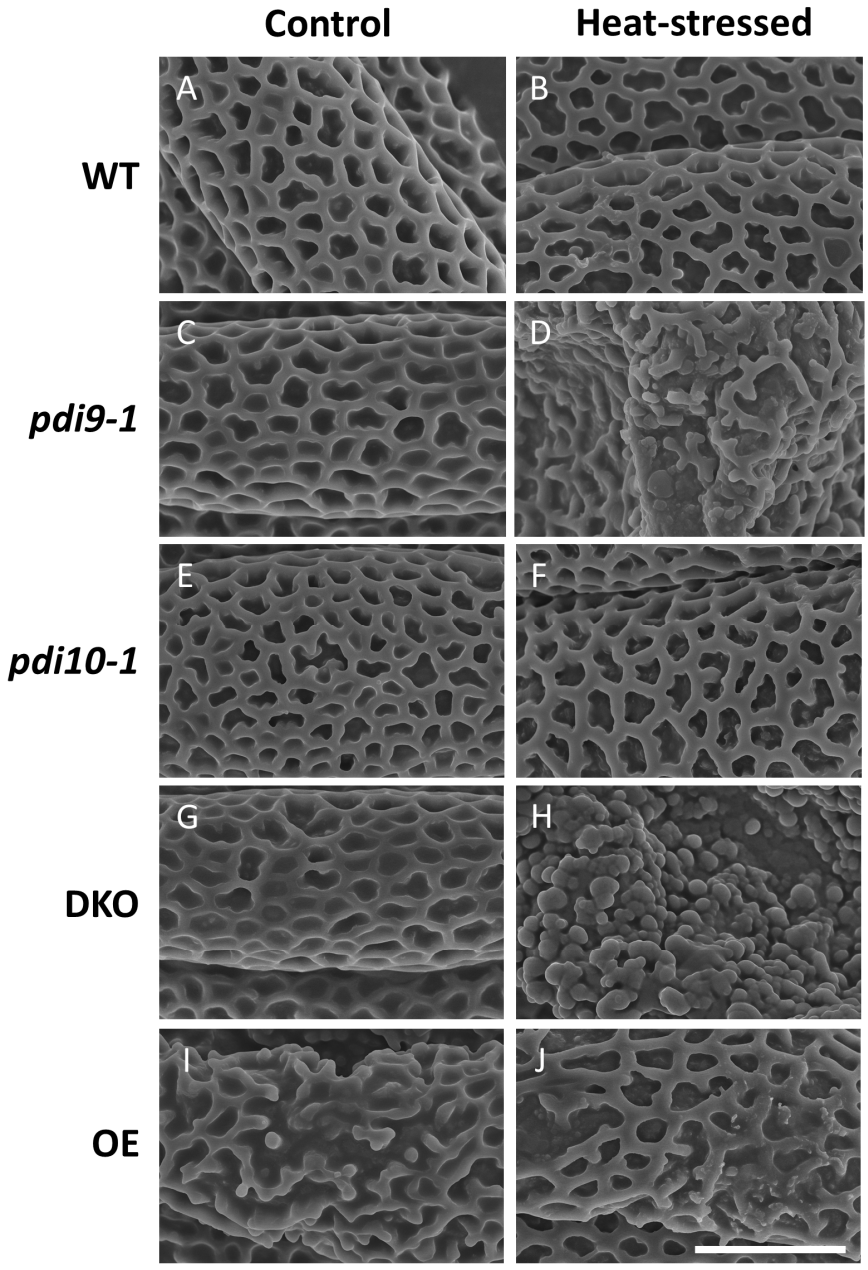

FIGURE 20: Scanning electron micrographs of pollen exine patterning. Each micrograph is a representative pollen grain from control (A,C,E,G,I) and heat-stressed (B,D,F,H,J) plants. Wild-type (A,B), *pdi9-1* (C,D), *pdi10-1* (E,F), DKO (G,H), and OE (I,J) pollen grains were all observed at 11,000X magnification. Scale bar is 5 um.

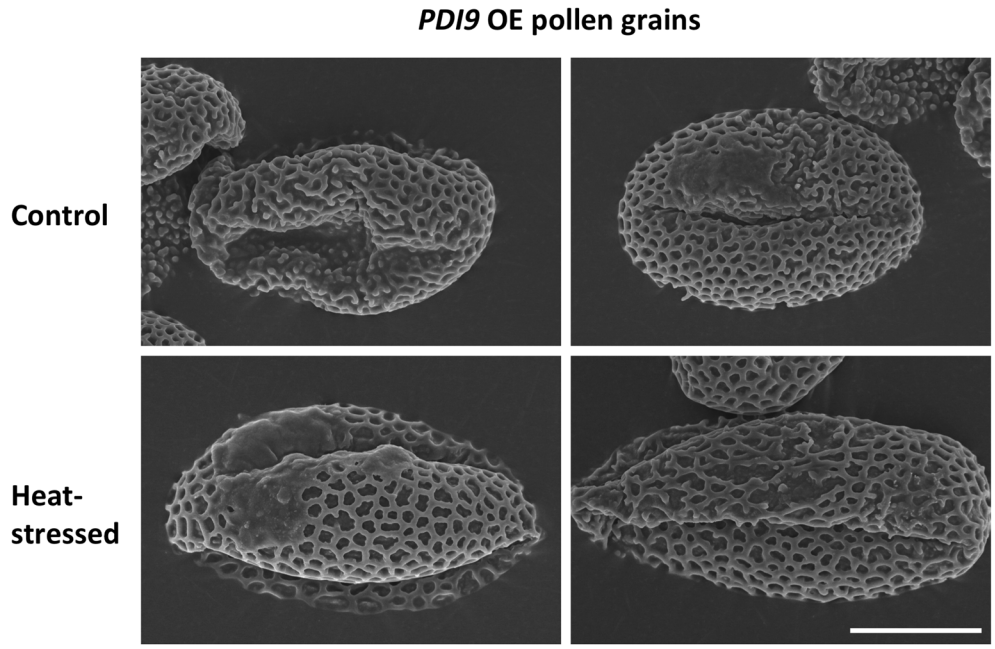

FIGURE 21: Addition scanning electron micrographs of representative *PDI9* OE pollen. Scale bar is 10 um.

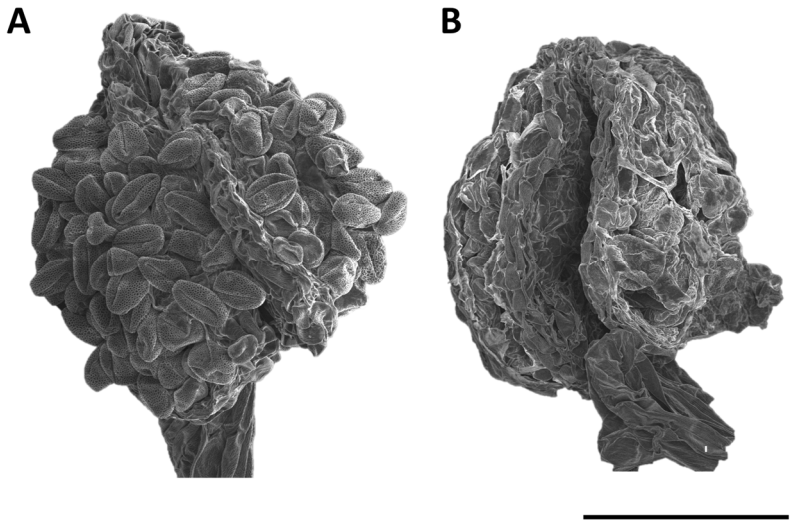

FIGURE 22: Representative anthers from (A) wild-type and (B) DKO heat-stressed flowers. Scale bar is 100 um.

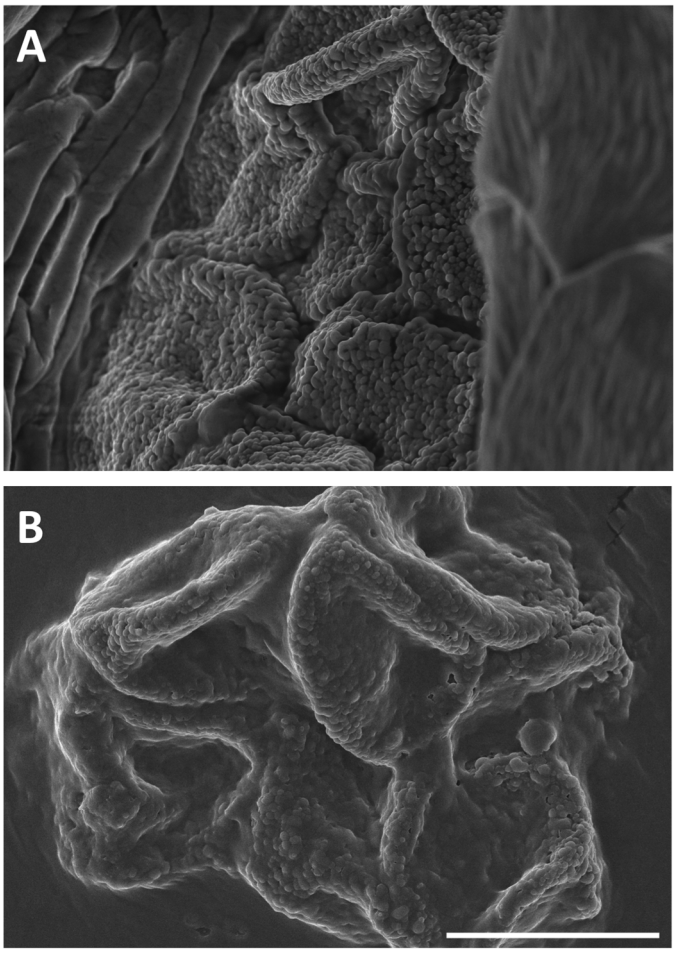

FIGURE 23: Heat-stressed DKO pollen within (A) anthers and (B) dehisced. Scale bar is 10 um.

Wild-type anthers under heat stress have dozens of mature, morphologically normal pollen grains ready to release, whereas DKO anthers are show no healthy pollen grains (Figure 22). In fact, deformed pollen grains are trapped within the anther. Figure 23A shows deformed pollen grains with an almost deflated football shape, with the unusual lumpy exine patterning. What little pollen that dehisced is shown Figure 23B; the micrograph of the deformed pollen

cluster is plausibly equivalent to the stained pollen cluster in Figure 17B. In summary, pollen development under heat stress is disrupted in the *pdi9* single knockout and exacerbated in the *pdi9-pdi10* double knockout.

Heat-stressed siliques

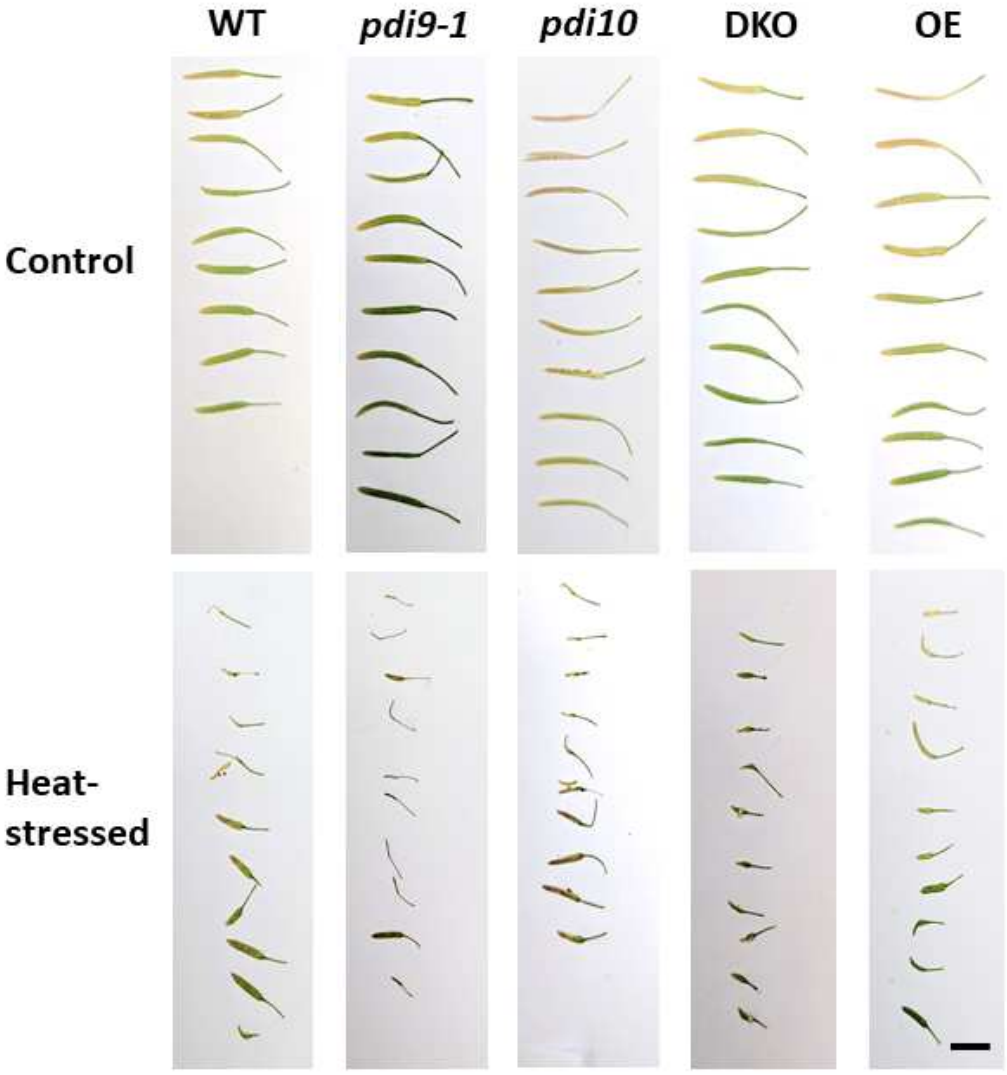

FIGURE 24: Representative siliques from control and heat-stressed plants. Scale bar is 5 mm.

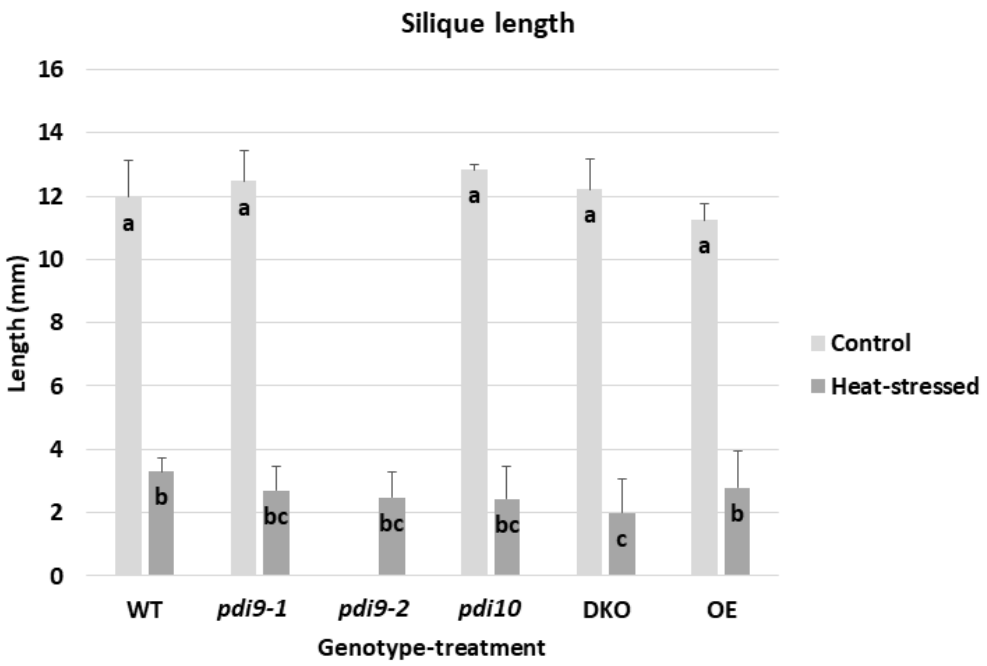

FIGURE 25: Silique length of control and heat-stressed plants. Letters indicate significance between samples ($p<0.05$ for n=3 control and n=6 heat-stressed plants).

Under heat stress, all genotypes show a reduction in viable pollen. Naturally, lower total pollen counts reduced viability result in fewer opportunities for fertilization. If viable pollen counts are sufficiently low, seed set and silique length will be negatively impacted. Indeed, all genotypes form shorter siliques during heat stress, as shown in Figures 24 and 25. The DKO has 40% shorter siliques than WT under heat stress. This is consistent with the hypothesis that reduced dehiscent pollen leads to fewer seeds. The *PDI9* OE is not significantly different from WT under heat stress, however.

Discussion

Pollen viability and pollen counts

Prolonged heat stress decreases pollen viability across the five *Arabidopsis* genotypes studied. The *pdi9* single knockout and DKO show a significantly lower viability under heat stress relative to wild-type. Overexpression of *PDI9* does not negatively impact pollen viability under heat stress. Therefore, *PDI9* is important for pollen viability under heat stress, but a surplus of *PDI9* does not provide a protective effect relative to wild-type pollen.

The *pdi9-pdi10* double knockout has a lower viability than the *pdi9* single KO under heat stress. Pollen viability in the *pdi10* single KO is slightly lower but not significantly different than wild-type. In the *pdi10* single KO, the presence of *PDI9* alone is sufficient to protect pollen development under heat stress. It's possible that *PDI10* protein in the *pdi9* single KO is capable of partially compensating for the role of *PDI9* in pollen development. It follows that the *pdi9-pdi10* double knockout is more susceptible to heat stress than both the *pdi9* and *pdi10* single knockouts. *PDI9* plays a crucial role in pollen development during heat stress that is partially, but not sufficiently, compensated by *PDI10*.

Pollen morphology and exine patterning

Scanning electron microscopy, alongside viability staining, sheds light on the timing and molecular impacts of *PDI9* on pollen development. Figures 22B and 23A demonstrate that *pdi9-pdi10* double KO is morphologically deformed and does not dehisce properly. Additionally, the pollen cell walls of the *pdi9-1* single KO and the double KO show improper exine patterning not found in wild-type. Taken together, *PDI9* knockout mutant pollen subjected to prolonged heat

stress has abnormal cell walls, is misshapen, less capable of dehiscence and ultimately less viable.

Surprisingly, the *PDI9* overexpressor pollen shows unusual exine patterning in both non-stressed and stressed conditions. The pattern is normal on the majority of the exine, but it was frequently observed to have small patches of disrupted reticulate exine. However, there is precedent in the literature for a UPR protein to have a homeostatic or "Goldilocks" level of expression in pollen. *Tunicamycin Induced 1 (TIN1)* is induced during ER stress, as its name suggests, and is abundant in pollen (Iwata et al. 2010). Both knockout *tin1* and 35S:TIN1 overexpressor pollen grains have an especially sticky pollen coat (Iwata et al. 2012; Iwata et al. 2017). The authors suggest that *TIN1* mutants have a defective ER quality control system in developing pollen, such that the misregulated secretion of proteins and perhaps lipids result in an abnormal pollen coat. In other words, there exists an amount of TIN1 in pollen that is "just right" for proper development. *PDI9* overexpression, *pdi9* knockout alone, and *pdi9-pdi10* double knockout all have reduced pollen counts and disrupted exine patterns. *PDI9* arguably fits this "Goldilocks" theory of proteostasis in pollen development.

Heat-stressed silique development

After discovering the *pdi9* pollen phenotype, a new question emerged: what are the downstream developmental impacts of decreased pollen viability under heat stress? Fewer pollen grains theoretically reduces the potential number of embryos, thereby reducing seed set. All genotypes showed a significant reduction in silique length, a metric for seed set, under heat stress. The *pdi9* and *pdi10* single knockouts did not show a difference in heat-stressed silique

length from wild-type, but the *pdi9-pdi10* double knockout had significantly shorter siliques under heat stress. Wang et al. (2017) found that triple and quadruple knockouts of *LRX8-LRX11* had shorter siliques with fewer seeds, resembling the DKO phenotype. Coupled with the co-localization data in Chapter III and the exine structure disruption in the stressed *pdi9* and *pdi9-pdi10* mutants, there is mounting evidence for an interaction between PDI9 and LRX8. Since LRX8 is anchored to the cell wall, it is most likely that PDI9 catalyzes the disulfide bonds between one or several of LRX8's thirteen cysteines as it passes through the ER. Said interaction is hypothetically important for the development of healthy pollen cell walls under heat stress. There are ongoing attempts to confirm the binding of PDI9 to LRX8 via co-immunoprecipitation.

Conclusions

The original aim of this thesis was to characterize the role of *PDI9* in pollen biogenesis. Wild-type and *PDI9* mutant pollen grains are not statistically different in non-stressed conditions. However, knockout plants lacking *PDI9* are more sensitive to heat stress. The exact molecular mechanisms underlying the changes in morphology and viability are not yet clear, but the most likely explanation is related to ER stress and an interaction with LRX8.

Tapetum development is fundamentally dependent on the secretion of proteins and nutrients to developing pollen. Anthers in non-stressed conditions exhibit higher protein folding demands than other tissues and in fact have up-regulation of UPR foldases and chaperones. The phenotypes documented here are not unlike the male reproductive phenotypes found for other UPR mutants. Specifically, *ire1a/ire1b* anthers are similar to wild-type anthers in non-stressed

conditions but show a significant reduction in viability and change in pollen coat composition; the *ire1a/ire1b* also have shorter siliques under heat stress (Deng et al. 2016). While *PDI9* knockout mutants may be capable of pollen development in non-stressed conditions, they are incapable of coping with the increased protein folding demand under heat stress. Moreover, *PDI9* may behave like its fellow UPR protein, *TIN1*, in that a specific balance is necessary for proper pollen development.

Finally, these findings suggest a possible role for *PDI9* homologs in crop yield under heat stress. *Arabidopsis thaliana* siliques are not unlike the fruits of important food crops like maize and rice. Further study is needed to confirm whether or not homologs of *PDI9* in other plant species play similar roles in pollen viability and silique length.

REFERENCES

Ahlers F, Lambert J, Wiermann R. 1999. Structural elements of sporopollenin from the pollen of Torreya californica torr. (Gymnospermae): using the H-1-NMR technique. Z. Naturforsch. Teil C 54:492–95.

Alberts B, Johnson A, Lewis J, et al. Molecular Biology of the Cell. 4th edition. New York: Garland Science; 2002. The Endoplasmic Reticulum.

Alexander MP. 1969. Differential Staining of Aborted and Nonaborted Pollen, Stain Technology, 44(3):117-122.

Angelos E and Brandizzi F. 2018. NADPH oxidase activity is required for ER stress survival in plants. Plant J 96: 1106-1120.

Ariizumi T and Toriyama K. 2011. Genetic Regulation of Sporopollenin Synthesis and Pollen Exine Development. Annual Review of Plant Biology 62(1): 437–460.

Aslund F, Beckwith J. 1999. The thioredoxin superfamily: redundancy, specificity, and gray-area genomics. *J Bacteriol*. 181(5): 1375-9.

Bagratuni T, Wu P, Gonzalez de Castro D, Davenport E L, Dickens N J, Walker B A, Boyd K, Johnson D C, Gregory W, Morgan G J, & Davies F E. 2010. XBP1s levels are implicated in the biology and outcome of myeloma mediating different clinical outcomes to thalidomide-based treatments. Blood 116(2): 250-253.

Bao Y, Bassham DC, Howell SH. 2019. A functional unfolded protein response is required for normal vegetative development. Plant Physiology preview. DOI: 10.1104/pp.18.01261.

Barela C and Smith T. 2016. PDI9 and PDI10 GUS and Western blot analysis. Unpublished.

Barnabás B, Jäger K, Fehér A. 2008. The effect of drought and heat stress on reproductive processes in cereals. Plant, Cell & Environment, 31:11-38.

Battat M, Eitan A, Rogachev I, Hanhineva K, Fernie A, Tohge T, Beekwilder J, Aharon A. 2019. A MYB Triad Controls Primary and Phenylpropanoid Metabolites for Pollen Coat Patterning. Plant Physiology preview. DOI: 10.1104/pp.19.00009.

Baumberger N, Ringli C, Keller B. 2001. The chimeric leucine-rich repeat/extensin cell wall protein LRX1 is required for root hair morphogenesis in Arabidopsis thaliana. Genes Dev. 15(9):1128-39.

Bella J, Hindlea K L, McEwanb P A, and Lovella S C. 2008. The leucine-rich repeat structure. Cell. Mol. Life Sci. 65: 2307 – 2333

Blobel G. 1980 Intracellular protein topogenesis. Proc Natl Acad Sci USA 77:1496–500.

Brunsing R, Omori A, Weber F, Bicknell A, Friend L, Rickert R, Niwa M. 2008. B- and T-cell Development Both Involve Activity of the Unfolded Protein Response Pathway. J. Biol. Chem. 283: 17954-61.

Bulaj G & Olivera BM. 2008. Folding of Conotoxins: Formation of the Native Disulfide Bridges During Chemical Synthesis and Biosynthesis of Conus Peptides. Antioxidants & Redox Signaling, 10(1), 141–156.

Bulaj G, Buczek O, Goodsell I, et al. 2003. Efficient oxidative folding of conotoxins and the radiation of venomous cone snails. Proc Natl Acad Sci USA 100(Suppl 2):14562-8.

Bulleid, N J. 2012. Disulfide Bond Formation in the Mammalian Endoplasmic Reticulum. Cold Spring Harbor Perspectives in Biology, 4(11), a013219.

Calfon M, Zeng H, Urano F, Till J H, Hubbard S R, Harding H P, Clark S G and Ron D. 2002. IRE1 couples endoplasmic reticulum load to secretory capacity by processing the XBP-1 mRNA. Nature 415: 92–96.

Carter B, Henderson JT, Svedin E, et al. 2016. Cross-Talk Between Sporophyte and Gametophyte Generations Is Promoted by CHD3 Chromatin Remodelers in Arabidopsis thaliana. Genetics 203(2):817-29.

Chang M and Huang S. 2017. Rapid Isolation of Total Protein from Arabidopsis Pollen. Bio-protocol 7(8): e2227.

Che P, Bussell JD, Zhou W, Estavillo GM, Pogson BJ, Smith SM. 2010. Signaling from the endoplasmic reticulum activates brassinosteroid signaling and promotes acclimation to stress in Arabidopsis. Sci Signal 3: ra69.

Chen X, Iliopoulos D, Zhang Q, et al. 2014. XBP1 Promotes Triple Negative Breast Cancer By Controlling the HIF1α Pathway. Nature 508(7494): 103-107.

Chen Y and Brandizzi F. 2012. AtIRE1A/AtIRE1B and AGB1 independently control two essential unfolded protein response pathways in Arabidopsis. The Plant J. 69: 266-277.

Chitwood PJ. Szymon J, Guna A, Shao S, Hegde RS. 2018. EMC Is Required to Initiate Accurate Membrane Protein Topogenesis. Cell 175:1507–1519.

Cho E J, Yuen C Y, Kang B-H, Ondzighi C, Staehelin L A, Christopher D A. 2011. Protein disulfide isomerase-2 of Arabidopsis mediates protein folding and localizes to both the secretory pathway and nucleus, where it interacts with maternal effect embryo arrest factor. Molecules and Cells 32:459-75.

Cifuentes-Esquivel N, Celiz-Balboa J, Henriquez-Valencia C, et al. 2018. bZIP17 regulates the expression of genes related to seed storage and germination, reducing seed susceptibility to osmotic stress. J Cell Biochem 119:6857–6868.

Cox JS, Shamu CE, Walter P. 1993. Transcriptional induction of genes encoding endoplasmic reticulum resident proteins requires a transmembrane protein kinase. Cell 73(6):1197-1206.

Deng Y, Srivastava R, Howell SH. 2013. Function of IRE1 in plant growth and development. Proceedings of the National Academy of Sciences 110(48):19633-19638.

Eletto D, Eletto D, Dersh D, Gidalevitz T, Argon Y. 2014. Protein Disulfide Isomerase A6 controls the decay of IRE1α signaling via disulfide-dependent association. Mol Cell. 53(4):562–576.

Ellgaard L, & Ruddock L W. 2005. The human protein disulphide isomerase family: substrate interactions and functional properties. EMBO Reports, 6(1), 28–32.

Erickson RR, Dunning LM, Olson DA, Cohen SJ, Davis AT, Wood WG, Kratzke RA, Holtzman JL. 2005. In cerebrospinal fluid ER chaperones ERp57 and calreticulin bind beta-amyloid. Biochem Biophys Res Commun. 332(1):50-7.

Fontes EB, Shank BB, Wrobel RL, et al. 1991. Characterization of an immunoglobulin binding protein homolog in the maize floury-2 endosperm mutant. Plant Cell. 3(5):483-96.

Forsthoefel N R, Dao T P and Vernon D M. 2010. PIRL1 and PIRL9, encoding members of a novel plant-specific family of leucine-rich repeat proteins, are essential for differentiation of microspores into pollen. Planta 232(5):1101-14.

Forsthoefel NR, Cutler K, Port MD, Yamamoto T, Vernon DM. 2005. PIRLs: a novel class of plant intracellular leucine-rich repeat proteins. Plant Cell Physiol 46:913–922.

Frand AR, Kaiser CA. 1998. The ERO1 gene of yeast is required for oxidation of protein dithiols in the endoplasmic reticulum. Mol Cell 1:161–170.

Freedman RB, Desmond JL, Byrne LJ, et al. 2017. 'Something in the way she moves': The functional significance of flexibility in the multiple roles of protein disulfide isomerase (PDI). Biochim Biophys Acta Proteins Proteom. 1865(11 Pt A):1383-1394.

Galligan J J, and Petersen D R. 2012.The human protein disulfide isomerase gene family. Human Genomics 6:6.

Gao H, Brandizzi F, Benning C, Larkin R M. 2008. A membrane-tethered transcription factor defines a branch of the heat stress response in Arabidopsis thaliana. Proceedings of the National Academy of Sciences Oct 2008, 105 (42) 16398-1640

Gething, M-J and Sambrook J. 1992. Protein folding in the cell. Nature 355:33-45.

Goldberg RB, Beals TP, Sanders PM. 1993. Anther development: basic principles and practical applications. Plant Cell, 5, 1217–1229.

Gruber C W, Čemažar M, Heras B, Martin J L, Craik D J. 2006. Protein disulfide isomerase: the structure of oxidative folding. Trends in Biochemical Sciences 31(8): 455-464.

Guna A, Volkmar N, Christianson JC, Hegde RS. 2018. The ER membrane protein complex is a transmembrane domain insertase. Science 359:470–473.

Hardy JA and Higgins GA. 1992. Alzheimer's disease: the amyloid cascade hypothesis. Science 256(5054): 184-185.

Henriquez-Valencia C , Moreno A A, Sandoval-Ibañez O, Mitina I, Blanco-Herrera F, Cifuentes-Esquivel N, and Orellana A. 2015. bZIP17 and bZIP60 Regulate the Expression of BiP3 and Other Salt Stress Responsive Genes in an UPR-Independent Manner in Arabidopsis thaliana. J. Cell. Biochem 116: 1638-1645.

Heslop-Harrison, J. 1968. Pollen Wall Development. Science 161(3838):230-237.

Hollien J and Weissman JS. 2006. Decay of Endoplasmic Reticulum-Localized mRNAs During the Unfolded Protein Response. Science 313(5783):104-107.

Honys D and Twell D. 2004. Transcriptome analysis of haploid male gametophyte development in Arabidopsis. Genome Biol. 5(11).

Houston N L, Fan C, Xiang Q-Y, Schulze J-M, Jung R and Boston R S. 2005. Phylogenetic Analyses Identify 10 Classes of the Protein Disulfide Isomerase Family in Plants, Including Single-Domain Protein Disulfide Isomerase-Related Proteins. Plant Physiol. 137: 762-778

Howell SH. 2017. When is the unfolded protein response not the unfolded protein response? Plant Science 260:139-143.

Hwang J and Qi L. 2018. Quality Control in the Endoplasmic Reticulum: Crosstalk between ERAD and UPR pathways. Trends in Biochemical Sciences 43(8): 593–605.

Inaba K and Ito K. 2008. Structure and mechanisms of the DsbB-DsbA disulfide bond generation machine. Biochim Biophys Acta. 1783(4):520-9.

Iwata Y, Fedoroff NV, Koizumi N. 2008. Arabidopsis bZIP60 is a proteolysis-activated transcription factor involved in the endoplasmic reticulum stress response. Plant Cell 20: 3107–312.

Iwata Y, Nishino T, Iwano M, Takayama S, Koizumi N. 2012. Role of the plant-specific endoplasmic reticulum stress-inducible gene TIN1 in the formation of pollen surface structure in Arabidopsis thaliana. Plant Biotechnology 29:51–56.

Iwata Y, Nishino T, Koizumi N. 2017. Overexpression of the endoplasmic reticulum stress-inducible gene TIN1 causes abnormal pollen surface morphology in Arabidopsis. Plant Biotechnology 34:173–176.

Iwata Y, Nishino T, Takayama S, Koizumi N. 2010. Characterization of a Plant-Specific Gene Induced by Endoplasmic Reticulum Stress in Arabidopsis thaliana. Bioscience, Biotechnology, and Biochemistry 74(10):2087-2091.

Jessop CE, Watkins RH, Simmons JJ, Tasab M, Bulleid NJ. 2009. Protein disulphide isomerase family members show distinct substrate specificity: P5 is targeted to BiP client proteins. J Cell Sci.122(23):4287-95.

Johnson-Brousseau S A, McCormick S. 2004. A compendium of methods useful for characterizing Arabidopsis pollen mutants and gametophytically-expressed genes. Plant J. 39(5):761-75.

Kawanabe T, Ariizumi T, Kawai-Yamada M, Uchimiya H, Toriyama K. 2006. Abolition of the Tapetum Suicide Program Ruins Microsporogenesis. Plant and Cell Physiology 47(6):784–787.

Kemmink J, Darby NJ, Dijkstra K, Nilges M, Creighton TE. 1997. The folding catalyst protein disulfide isomerase is constructed of active and inactive thioredoxin modules. Curr Biol 7:239–245.

Kim H, Bhattacharya A, Qi L. 2015. Endoplasmic reticulum quality control in cancer: friend or foe. Seminars in cancer biology 33:25-33.

Kim J-S, Yamaguchi-Shinozaki K, Shinozaki K. 2018. ER-Anchored Transcription Factors bZIP17 and bZIP28 Regulate Root Elongation. Plant Physiology 76(3):2221-2230.

Kobe B and Deisenhofer J. 1994. The leucine-rich repeat: a versatile binding motif. Trends Biochem Sci 19:415–421.

Krug MS and Berger SL. 1987. First strand cDNA synthesis primed with oligo(dT). Methods in Enzymology 152: 316-324.

Lai YS, Stefano G, Zemelis-Durfee S, Ruberti C, Gibbons L, and Brandizzi F. 2018. Systemic signaling contributes to the unfolded protein response of the plant endoplasmic reticulum. Nature Communications 9:3918.

Lamport D T A, Kieliszewski M J, Chen Y, and Cannon M C. 2011. Role of the Extensin Superfamily in Primary Cell Wall Architecture. Plant Physiol. 156: 11-19.

Lee E and Lee DH. 2017. Emerging roles of protein disulfide isomerase in cancer. *BMB Rep*. 50(8):401–410.

Lenny N and Green M. 1991. Regulation of Endoplasmic Reticulum Stress Proteins in COS Cells Transfected with Immunoglobulin p Heavy Chain cDNA. J. Biol. Chem 266(30): 20532-20537.

Li DD, Xue JS, Zhu J, Yang ZN. 2017. Gene Regulatory Network for Tapetum Development in Arabidopsis thaliana. Front Plant Sci. 8:1559.

Lippincott-Schwartz J, Roberts TH, Hirschberg K. 2000. Secretory Protein Trafficking and Organelle Dynamics in Living Cells. Annual Review of Cell and Developmental Biology 16(1): 557–589.

Liu JX, Howell SH. 2010. bZIP28 and NF-Y transcription factors are activated by ER stress and assemble into a transcriptional complex to regulate stress response genes in Arabidopsis. Plant Cell 22(3):782-96.

Liu JX, Srivastava R, Che P, and Howell SH. 2007b. An endoplasmic reticulum stress response in Arabidopsis is mediated by proteolytic processing and nuclear relocation of a membrane-associated transcription factor, bZIP28. Plant Cell 19: 4111–4119.

Liu JX, Srivastava R, Che P, Howell SH. 2007a. Salt stress responses in Arabidopsis utilize a signal transduction pathway related to endoplasmic reticulum stress signaling. Plant J. 51(5):897-909.

Lu D-P, Christopher DA. 2008. Endoplasmic reticulum stress activates the expression of a sub-group of protein disulfide isomerase genes and AtbZIP60 modulates the response in Arabidopsis thaliana. Molecular Genetics & Genomics 280:199-210.

Lu D-P, Christopher DA. 2008. Light enhances the unfolded protein response as measured by BiP2 gene expression and the secretory GFP-2SC marker in *Arabidopsis*. *Physiologia Plantarum*, 134: 360–368.

Ludwig-Muller J, Krishna P, and Forreiter C. 2000. A Glucosinolate Mutant of Arabidopsis Is Thermosensitive and Defective in Cytosolic Hsp90 Expression after Heat Stress. Plant Physiol. 123: 949-958.

Malhotra JD, Kaufman RJ. The Endoplasmic Reticulum and the Unfolded Protein Response. Seminars in cell & developmental biology. 2007;18(6):716-731. doi:10.1016/j.semcdb.2007.09.003.

Martínez-García J F, Monte E, Quail P H. 1999. A simple, rapid and quantitative method for preparing Arabidopsis protein extracts for immunoblot analysis. Plant J 20(2): 251-257.

Maruyama D, Sugiyama T, Endo T, Nishikawa S-I. 2014. Multiple BiP genes of Arabidopsis thaliana are required for male gametogenesis and pollen competitiveness. Plant Cell Physiol 55:801–810.

Maruyama K , Ogata T , Kanamori N, Yoshiwara K, Goto S, Yamamoto Y Y, Tokoro Y, Noda C, Takaki Y, Urawa H, Iuchi S, Urano K, Yoshida T, Sakurai T, Kojima M, Sakakibara H, Shinozaki K and Yamaguchi□Shinozaki K. 2017. Design of an optimal promoter involved in the heat-induced transcriptional pathway in Arabidopsis, soybean, rice and maize. Plant J 89: 671-680.

Merksamer PI, Trusina A, Papa FR. Real-time redox measurements during endoplasmic reticulum stress reveal interlinked protein folding functions. Cell. 2008;135(5):933-47.

Michaely P and Bennett V. 1995. Mechanism for Binding Site Diversity on Ankyrin: Comparison of binding sites on ankyrin for neurofascin and the Cl/HCO3 anion exchanger. J Biol Chem 270: 31298-31302.

Mishiba K, Nagashima Y, Suzuki E, Hayashi N, Ogata Y, Shimada Y, Koizumi N. 2013. Defects in IRE1 enhance cell death and fail to degrade mRNAs encoding secretory pathway proteins in the Arabidopsis unfolded protein response. Proc Natl Acad Sci 110(14):5713-8.

Nagashima Y, Mishiba K, Suzuki E, Shimada Y, Iwata Y, Koizumi N. 2011. Arabidopsis IRE1 catalyses unconventional splicing of bZIP60 mRNA to produce the active transcription factor. Scientific Reports 1:29.

Nelson BK, Cai X, and Nebenführ A. 2007. A multi-color set of in vivo organelle markers for colocalization studies in Arabidopsis and other plants. Plant Journal 51:1126-1136.

Nishikawa S, Zinkl G M, Swanson R J, Maruyama D, and Preuss D. 2005. Callose (β-1,3 glucan) is essential for Arabidopsis pollen wall patterning, but not tube growth. BMC Plant Biology 5(22).

Nørgaard P, Westphal V, Tachibana C, Alsøe L, Holst B, Winther JR. 2001. Functional differences in yeast protein disulfide isomerases. *J Cell Biol*. 152(3):553-62.

O'Brien H, Kanemura S, Okumura M, Baskin RP, Bandyopadhyay PK, Olivera BM, Ellgaard L, Inaba K, Safavi-Hamami H. 2018. Ero1-Mediated Reoxidation of Protein Disulfide Isomerase Accelerates the Folding of Cone Snail Toxins. Int. J. Mol. Sci. 19: 3418.

Ondzighi C A, Christopher D A, Cho E J, Chang S C, Staehelin L A. 2008. Arabidopsis Protein Disulfide Isomerase-5 Inhibits Cysteine Proteases during Trafficking to Vacuoles before Programmed Cell Death of the Endothelium in Developing Seeds. The Plant Cell 20:2205-2220.

Pacini E, Franchi GG, Hesse M. 1985. The Tapetum: Its Form, Function, and Possible Phylogeny in Embryophyta. Plant Systematics and Evolution 149(3): 155-185.

Perri ER, Thomas CJ, Parakh S, Spencer DM, Atkin JD. 2016. The Unfolded Protein Response and the Role of Protein Disulfide Isomerase in Neurodegeneration. Frontiers in Cell and Developmental Biology 3:80.

Peterson R, Slovin JP, Chen C. 2010. A simplified method for differential staining of aborted and non-aborted pollen grains. International Journal of Plant Biology 1:e13.

Pihlajaniemi T, Helaakoski T, Tasanen K, Myllylä R, Huhtala M L, Koivu J, & Kivirikko K I. 1987. Molecular cloning of the beta-subunit of human prolyl 4-hydroxylase. This subunit and protein disulphide isomerase are products of the same gene. The EMBO Journal, 6(3), 643–649.

Pirneskoski A, Klappa P, Lobell M, Williamson RA, Byrne L, Alanen HI, Salo KE, Kivirikko KI, Freedman RB, Ruddock LW. 2004. Molecular characterization of the principal substrate binding site of the ubiquitous folding catalyst protein disulfide isomerase. J Biol Chem. 279(11):10374-81.

Porter B W, Yuen C Y L, Christopher D A. 2015. Dual protein trafficking to secretory and non-secretory cell compartments: Clear or double vision? Plant Science, 234: 174-179.

Puillandre N, Watkins M, Olivera BM. 2010. Evolution of Conus peptide genes: duplication and positive selection in the A-superfamily. J Mol Evol. 70(2):190-202.

Qin Y, Leydon AR, Manziello A, Pandey R, Mount D, Denic S, et al. 2009. Penetration of the Stigma and Style Elicits a Novel Transcriptome in Pollen Tubes, Pointing to Genes Critical for Growth in a Pistil. PLoS Genet 5(8)

Radja A, Horsley EM, Lavrentovich MO, Sweeney AM. 2019. Pollen Cell Wall Patterns Form from Modulated Phases. Cell 176:856–868.

Rao RV, Bredesen DE. 2004. Misfolded proteins, endoplasmic reticulum stress and neurodegeneration. Curr Opin Cell Biol 16(6):653-62.

Richard M, Boulina T, Roberta VJP, Richmond JE, Bessereaua JL. 2013. Biosynthesis of ionotropic acetylcholine receptors requires the evolutionarily conserved ER membrane complex. PNAS 110(11):E1055-E1063.

Ron D and Walter P. 2007. Signal integration in the endoplasmic reticulum unfolded protein response. Nat Rev Mol Cell Biol 8:519–529.

Rosenzweig C, Elliott J, Deryng D, et al. 2013. Assessing agricultural risks of climate change in the 21st century in a global gridded crop model intercomparison. Proc Natl Acad Sci U S A 111(9):3268-73.

Russell SJ, Ruddock LW, Salo KE, Oliver JD, Roebuck QP, Llewellyn DH, Roderick HL, Koivunen P, Myllyharju J, High S. 2004. The primary substrate binding site in the b' domain of ERp57 is adapted for endoplasmic reticulum lectin association. J Biol Chem 279(18):18861-9.

Sede AR, Borassi C, Wengier DL, Mecchia MA, Estevez JM, Muschietti JP. 2018. Arabidopsis pollen extensins LRX are required for cell wall integrity during pollen tube growth. FEBS Letters 592:233-243.

Selles B, Jacquot JP, Rouhier N. 2011. Comparative genomic study of protein disulfide isomerases from photosynthetic organisms. Genomics 97:37–50

Showalter, A M. 1993. Structure and Function of Plant Cell Wall Proteins. The Plant Cell Online, 5(1): 9–23.

Smyth DR, Bowman JL, Meyerowitz EM. 1990. Early flower development in Arabidopsis. The Plant Cell 2:755-767.

Tan F, Zhu H, He X, et al. 2018. Role of TXNDC5 in tumorigenesis of colorectal cancer cells: In vivo and in vitro evidence. Int J Mol Med. 2018;42(2):935-945.

Tohda C, Urano T, Umezaki M, Nemere I, Kuboyama T. Diosgenin is an exogenous activator of 1,25D-MARRS/Pdia3/ERp57 and improves Alzheimer's disease pathologies in 5XFAD mice. Sci Rep. 2:535.

United Nations, Department of Economic and Social Affairs, Population Division. 2017. World Population Prospects: The 2017 Revision, Key Findings and AdvanceTables. Working Paper No. ESA/P/WP/248.

Van Dalfsen KM, Hodapp S, Keskin A, …, Nomura DK, Jovanovic M, Barr GA. 2018. Global Proteome Remodeling during ER Stress Involves Hac1-Driven Expression of Long Undecoded Transcript Isoforms. Developmental Cell 46:219–235.

Verma DP, Hong Z. 2001. Plant callose synthase complexes. Plant Mol. Biol. 47:693–701.

Wang C, Li W, Ren J, Fang J, Ke H, Gong W, Feng W, and Wang CC. 2013. Structural insights into the redox-regulated dynamic conformations of human protein disulfide isomerase. Antioxid Redox Signal 19(1):36-45.

Wang H, Boavida LC, Ron M, McCormick S. 2008. Truncation of a protein disulfide isomerase, PDIL2–1, delays embryo sac maturation and disrupts pollen tube guidance in Arabidopsis thaliana. Plant Cell 20:3300–3311

Wang X, Chen J, Liu C, Luo J, Yan X, Ai A, Cai Y, Xie H, Ding X, Peng X. 2019. Over-expression of a protein disulfide isomerase gene from Methanothermobacter thermautotrophicus enhances heat stress tolerance in rice. Gene 684: 124-130.

Wang X, Wang K, Yin G, Liu X, Liu M, Cao N, Duan Y, Gao H, Wang W, Ge W, Wang J, Li R, and Guo Y. 2018. Pollen-Expressed Leucine-Rich Repeat Extensins Are Essential for Pollen Germination and Growth. Plant Physiology 176(3): 1993-2006.

Wideman J. 2015. The ubiquitous and ancient ER membrane protein complex (EMC): Tether or not?. F1000Research. 4.

Wilson R, Lees J F, Bulleid N J, 1998.Protein disulfide isomerase acts as a molecular chaperone during the assembly of procollagen. J Biol Chem 273(16):9637-43.

Worden N, Park E. and Drakakaki G. 2012. Trans-Golgi Network—An Intersection of Trafficking Cell Wall Components. Journal of Integrative Plant Biology, 54: 875–886

Worrall D, Hird DL, Hodge R, Paul W, Draper J, Scott R. 1992. Premature dissolution of the microsporocyte callose wall causes male sterility in transgenic tobacco. Plant Cell 4:759–71.

Xu J, Ding Z, Vizcay-Barrena G, Shi J, Liang W, Yuan Z, Werck-Reichhart D, Schreiber L, Wilson ZA, Zhang D. 2014. ABORTED MICROSPORES acts as a master regulator of pollen wall formation in Arabidopsis. Plant Cell 26:1544–1556.

Yang K , Xia C, Liu X, Dou X, Wang W, Chen L, Zhang X, Xie L, He L, Ma X and Ye D. 2009. A mutation in THERMOSENSITIVE MALE STERILE 1, encoding a heat shock protein with DnaJ and PDI domains, leads to thermosensitive gametophytic male sterility in Arabidopsis. The Plant Journal 57: 870-882.

Yuen C, Matsumoto K, and Christopher D A. 2013. Variation in the Subcellular Localization and Protein Folding Activity among Arabidopsis thaliana Homologs of Protein Disulfide Isomerase. Biomolecules 3: 848-869

Yuen C, Shek R, Kang B-H, Matsumoto K, Cho E J, and Christopher D A. 2016. Arabidopsis protein disulfide isomerase-8 is a type I endoplasmic reticulum transmembrane protein with thiol-disulfide oxidase activity. BMC Plant Biology 16:181.

Zhang XL, Ren YJ, and Zhao J. 2008. Roles of extensins in cotyledon primordium formation and shoot apical meristem activity in Nicotiana tabacum. Journal of Experimental Botany 59(14): 4045–4058.

Zhu J, Lou Y, Xu X, Yang ZN. 2011. A genetic pathway for tapetum development and function in Arabidopsis. J. Integr. Plant Biol. 53:892–900.

Zinkl GM, Zwiebel BI, Grier DG, Preuss D. 1999. Pollen–stigma adhesion in Arabidopsis: a species specific interaction mediated by lipophilic molecules in the pollen exine. Development 126:5431–40.

Zinn KE, Tunc-Ozdemir M, Harper JF. 2010. Temperature stress and plant sexual reproduction: uncovering the weakest links. J Exp Bot. 61(7):1959-68.

APPENDIX: LIST OF PRESENTATIONS

Feldeverd E and Christopher DA. 2018. Studies defining the role of protein disulfide isomerase-9, PDI9, in pollen biogenesis in Arabidopsis thaliana. North American Mass Spectrometry Summer School, University of Wisconsin Madison. Poster Presentation.

Feldeverd E. 2018. Protein disulfide isomerase-9 mediates the development of healthy pollen under environmental stress. CTAHR Student Research Symposium, University of Hawai‘i at Mānoa. Oral Presentation. Awarded Master of Science Oral 30th Anniversary (1st place).

Feldeverd E. 2018. Protein disulfide isomerase-9 mediates the development of healthy pollen under environmental stress. CTAHR Three Minute Elevator Pitch (3MEP), University of Hawai‘i at Mānoa. Oral Presentation.

Feldeverd E and Christopher DA. 2017. Studies defining the role of protein disulfide isomerase-9, PDI9, in pollen biogenesis in Arabidopsis thaliana. CTAHR Student Research Symposium, University of Hawai‘i at Mānoa. Poster Presentation.